

---

# SiT: Symmetry-Invariant Transformers for Generalisation in Reinforcement Learning

---

Matthias Weissenbacher<sup>1</sup> Rishabh Agarwal<sup>\*2</sup> Yoshinobu Kawahara<sup>\*13</sup>

## Abstract

An open challenge in reinforcement learning (RL) is the effective deployment of a trained policy to new or slightly different situations as well as semantically-similar environments. We introduce **Symmetry-Invariant Transformer (SiT)**, a scalable vision transformer (ViT) that leverages both local and global data patterns in a self-supervised manner to improve generalisation. Central to our approach is Graph Symmetric Attention, which refines the traditional self-attention mechanism to preserve graph symmetries, resulting in invariant and equivariant latent representations. We showcase SiT’s superior generalization over ViTs on MiniGrid and Procgen RL benchmarks, and its sample efficiency on Atari 100k and CIFAR10.

## 1. Introduction

Despite recent advances in reinforcement learning, out-of-distribution generalization remains an open challenge. A widely-used approach to improve generalisation in image-based RL is data augmentation (Hansen & Wang, 2021; Laskin et al., 2020; Yarats et al., 2021b) but it can lead to over regularisation to specific augmentations. Moreover, data augmentation’s inherent non-determinism can amplify the variance in regression targets, which can be detrimental to learning (Hansen et al., 2021). Complimentary to data augmentation, leveraging symmetries can improve generalization and lead to sample-efficient RL (Tang & Ha, 2021; Van der Pol et al., 2020; Weissenbacher et al., 2022).

Image-based RL may benefit from both local and global symmetries, which preserve a particular structure or prop-

erty within a neighborhood of a pixel or image patches and throughout the entire image respectively. Enforcing local symmetries through data augmentation is sample inefficient and computationally expensive. When an image is divided into local patches to capture these symmetries, the number of augmented samples we may need to represent all possible variations grows exponentially. Given the prevalence of symmetries in RL settings, it is advantageous for neural networks to possess the capability to develop a understanding of these local and global symmetries in a self-supervised manner that is data-driven.

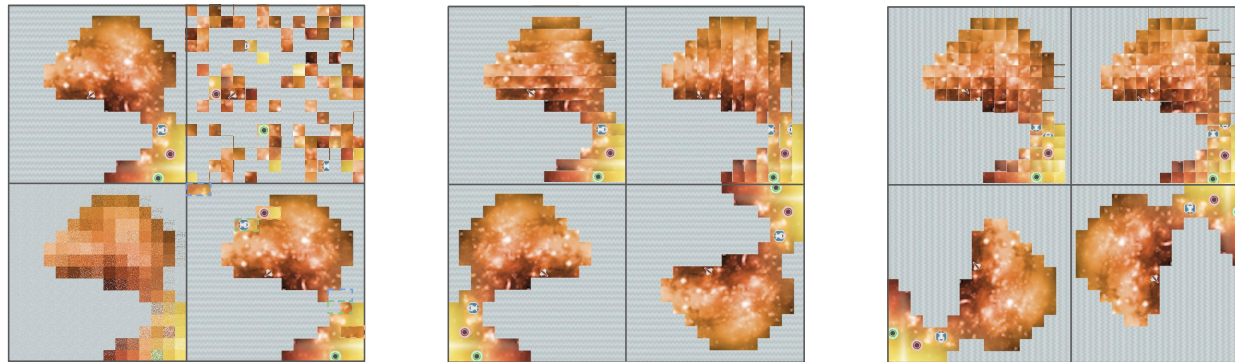
However, leveraging symmetries in RL presents various challenges. In particular, an agent’s action choices in general are not invariant under symmetries both globally and locally, see Figure 1. Permutation invariance (Tang & Ha, 2021) in Figure 1 (a) admits the shortcoming that it leads to dead-end situations in many settings, while local and global flip symmetries (b) inter-changes left /right and up / down actions. Moreover, in many scenarios, it’s essential for a decision-making process to consider the local context within the broader global setting, e.g., in Figure 1 (c), the global 90° rotation is an exact symmetry but local patch-wise rotations change the neighbourhood of the agent. In contrast, even minimal permutations are fatal for learning, see Figure 1 (a) bottom-right. This situation is common amongst many games and real-world environments (Bellemare et al., 2012; 2020; Cobbe et al., 2020; Kitano et al., 1997; Silver et al., 2016).

To address the aforementioned challenges, we present a self-attention based network architecture, which we call **Symmetry-invariant Transformer (SiT)**. SiTs incorporates a flexible relational inductive bias (Battaglia et al., 2018) to recognize relational patterns or symmetries, enabling it to adapt effectively to unfamiliar or out-of-distribution data. In addition to invariance, SiTs account for dead-end situations by incorporating equivariance, which refers to the property of an action to transform equivalently as the states under symmetries in our SiT module and by introducing a rotation symmetry preserving but flip-symmetry breaking layer. Additionally, we introduce novel invariant as well as equivariant **Graph Symmetric Attention (GSA)**. GSA is akin to self-attention of Vision Transformers (ViTs) (Doso-

---

<sup>\*</sup>Advisory role <sup>1</sup>RIKEN Center for Advanced Intelligence Project, Tokyo, Japan <sup>2</sup>Google DeepMind <sup>3</sup>Graduate School of Information Science and Technology, Osaka University, Japan. Correspondence to: Matthias Weissenbacher <wb-matthias@gmail.com>.

Accepted to be published in the Proceedings of the 41<sup>st</sup> International Conference on Machine Learning, Vienna, Austria. Copyright 2024 by the authors.



(a) Original (top-left) vs. patch and pixel-wise permutations. Permutation result in non-solvable domains; e.g. permuting 6 individual patches (bottom-right).

(b) Horizontal and vertical flips; patch-wise (top) - entire image (bottom). Approximate symmetry as it breaks left / right actions.

(c) Left and right rotations by  $90^\circ$ . Patch-wise (top): agent's local neighbourhood altered; Entire image: global exact symmetry (bottom).

Figure 1. Local (patch-wise) and global transformations of observations of the CaveFlyer environment, Procgen suite (Cobbe et al., 2020). Permutation invariant agents (Tang & Ha, 2021) can't discern key features (a) in contrast to agents with local and/or global flip and rotation invariance (b) and (c).

vitskiy et al., 2020), by adapting permutation-invariant self-attention (Lee et al., 2019) to maintain graph symmetries.

SiTs capitalize on the interplay between local and global information. This is achieved by incorporating both local and global GSA modules. In particular, the local attention window stretches over several image patches, such that the local symmetries do not change the agent's local broader neighbourhood. We demonstrate the efficacy of SiTs over ViTs on prevalent RL generalization benchmarks, namely MiniGrid and Procgen, and show sample-efficiency on the the Atari100k and CIFAR-10 vision benchmark.

In summary, our contribution is fourfold. First, we introduce a scalable invariant / equivariant transformer architecture (SiT), i.e. accounting for symmetries down to the pixel level (Section 4). Second, we perform empirical model evaluation on RL tasks; in contrast to conventional ViTs, SiTs require less hyper-parameter tuning, generalise better in RL tasks and are more sample-efficient. Specifically, SiTs lead to a  $3\times$  and  $9\times$  improvement in performance on commonly-used MiniGrid and Procgen environments. Third, SiTs incorporate a novel method to account for the interplay of local and global symmetries, which is complementary to widely-used data augmentation in image-based RL. Fourth, GSA is a novel approach to accomplish graph-symmetries in self-attention, not relying on positional embeddings (Fuchs et al., 2020; Romero & Cordonnier, 2021). We open sourced the SiT model-code on [GitHub](#).

## 2. Background

**Reinforcement Learning.** A Markov Decision Process (MDP) is a mathematical framework for modeling decision-making problems in stochastic environments. MDPs are

characterized by a tuple  $(\mathcal{S}, \mathcal{A}, \mathcal{P}, \mathcal{R}, \gamma)$ , where  $\mathcal{S}$  is a finite set of states,  $\mathcal{A}$  is a finite set of actions,  $\mathcal{P}$  is the transition probability function,  $\mathcal{R}$  is the reward function, and  $\gamma \in [0, 1)$  is the discount factor. In RL, one aims to learn optimal decision-making policies in MDPs. A policy, denoted as  $\pi : \mathcal{S} \rightarrow \mathcal{A}$ , is a mapping from states to actions. The optimal policy  $\pi$  maximizes the expected cumulative discounted reward, given by the value function  $V^\pi(s) = \mathbb{E}[\sum_{t=0}^{\infty} \gamma^t \mathcal{R}(s_t, a_t) \mid s_0 = s, a_t \sim \pi(\cdot \mid s_t)]$ , where the expectation is taken over the sequence of states and actions encountered by following the policy  $\pi$ . The optimal policy  $\pi^*$  is the one that satisfies  $V^{\pi^*}(s) \geq V^\pi(s)$  for all  $s \in \mathcal{S}$  and any other policy  $\pi$ .

**Invariance and Equivariance.** Invariance and equivariance are foundational concepts in understanding how functions respond to symmetries of their inputs. In RL, equivariance and invariance properties are imposed on the actor and value networks, e.g. in (Wang et al., 2023) on top of SAC (Haarnoja et al., 2018). Before defining these concepts, we introduce some notation. The function  $f$  maps elements from space  $\mathcal{S}$  to  $\mathcal{S}'$  and  $g$  denotes an individual transformation in a symmetry group. The functions  $\rho(g)$  and  $\rho'(g)$  describe the action of  $g$  on spaces  $\mathcal{S}$  and  $\mathcal{S}'$ , respectively, e.g.  $\rho(g) \cdot s$  signifies applying a transformation  $\rho(g)$  on an element  $s$  of  $\mathcal{S}$ .

*Invariance:* A function  $f$  is invariant with respect to a set of transformations (symmetry group) if the application of any transformation from this set to its input does not change the function's output. Mathematically, this is expressed as:  $f(\rho(g) \cdot s) = f(s)$  for every transformation  $g$ . *Equivariance:* A function  $f$  is equivariant if, when a transformation is applied to its input, there is a corresponding and predictable transformation of its output. This relationship is

captured by the equation:  $f(\rho(g) \cdot s) = \rho'(g) \cdot f(s)$  for every transformation  $g$  in the symmetry group.

**Attention mechanisms.** Recently, conventional self-attention have been employed in the context of RL agents (Tang & Ha, 2021). The permutation invariant self-attention layer (Lee et al., 2019) uses a fixed Q-matrix (queries). The original ViT architecture (Dosovitskiy et al., 2020) naturally admits permutation invariance (PI) due to use of token embeddings. PI is only broken by using the positional embedding (Fuchs et al., 2020; Romero & Cordonnier, 2021). The standard attention is given by

$$\text{Att}(K, V, Q) = \text{softmax}\left(\frac{1}{\sqrt{d_f}} Q K^T\right) V, \quad (1)$$

where  $K$ ,  $V$ , and  $Q$  denote the keys, values, and queries respectively. They are derived from the input  $X$ :  $K = XW^k$ ,  $V = XW^v$ ,  $Q = XW^q$ , where  $W^q$ ,  $W^k$ , and  $W^v$  are the corresponding weight matrices. The keys and values are constructed based on the input data, which is segmented into  $P$  patches. Consequently, the matrices  $K$ ,  $V$ , and  $Q$  have dimensions  $\mathbb{R}^{P \times d_f}$ , where  $d_f$  represents the feature dimension for each patch.

Graph neural networks and graph attention have been extensively explored in terms of their symmetries (Satorras et al., 2021b; Veličković et al., 2018). At a high-level, the graph attention mechanism (GAT) determines the relationships between nodes in a graph using attention. The attention matrix equation 1 is masked with the adjacency matrix  $\mathcal{G}$  to ensure that the attention coefficients are only computed for nodes that are connected in the graph

$$\text{GAT}(K, V, Q) = \text{softmax}\left(\frac{1}{\sqrt{d_f}} Q K^T\right) \mathcal{G} V, \quad (2)$$

with  $K, V, Q$  being the feature vectors of the nodes, multiplied with weight matrices. A symmetrisation of the score matrix may be added.<sup>1</sup> to ensure that connections between nodes are bidirectional, meaning their importance is consistent regardless of direction.

### 3. GSA: Symmetry-Invariant and Equivariant Attention

In this work, we propose a modification of the permutation invariant attention layer (Lee et al., 2019). This adaptation is specifically designed to respect the inherent symmetries of a square two-dimensional grid, which serves as our underlying graph structure. These symmetries include translations, rotations, and flips, as depicted in Figure 2. Our approach is an evolution of the rotary embedding method (Su et al.,

<sup>1</sup>Symmetrisation over the node / vertex indices given by  $\text{symmetric}(M) = M_{ij} + M_{ji}$  for  $i, j = 1, \dots, P$  for a square matrix  $M \in \mathbb{R}^{P \times P}$ .

2021). Our Graph Symmetric Attention (GSA) layer is conceptually similar to a traditional graph-adjacency matrix. Our graph topology matrix  $G$  is the analog of the adjacency matrix in equation 2; however, its trainable weights are uniquely constrained to abide by certain symmetry conditions, which we discuss later. While our discussion centers on the 2D grid, GSA may be adapted to 1D data where it ensures shift-symmetry (optionally flip-symmetry), see A.1.

For clarity, imagine a  $9 \times 9$  pixel image. When segmented into  $3 \times 3$  pixel patches, we get 9 distinct patches. In the **local** GSA setup, each graph vertex corresponds to an individual pixel, suggesting that in Figure 2, the term "patches" is synonymous with pixels. In contrast, the **global** GSA interprets the image as a collection of  $3 \times 3$  patches, where each patch's central point is symbolized by a graph vertex, aligning with the conventional ViT perspective. Taking inspiration from self-attention in graphs, we propose Graph Symmetric Attention (GSA):

$$\text{GSA}(K, V, Q) = \text{softmax}\left(\frac{1}{\sqrt{d_f}} \Gamma(Q, K)\right) G_v V \quad (3)$$

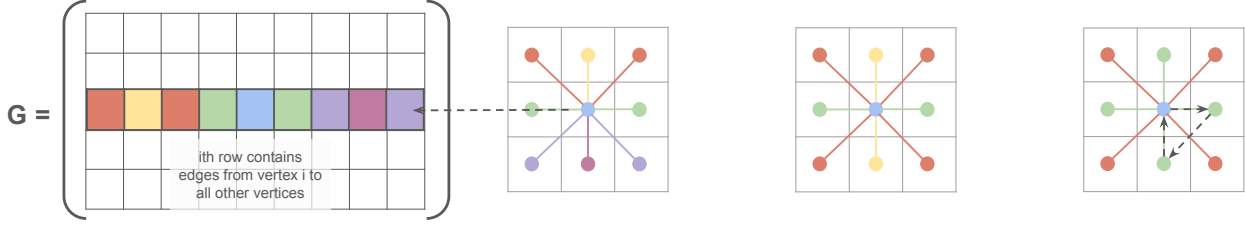
with the attention score matrix given by

$$\Gamma(Q, K) = \text{symmetric}\left(\left(G_q Q [G_k K]^T\right) \odot G\right),$$

where  $\odot$  is the point-wise Hadamard product. Here,  $\Gamma$  is interpreted as the attention graph matrix of the underlying 2D pixel grid. Analogous to equation 2, the grid symmetries are imposed by a graph topology matrix  $G$  which breaks permutation invariance of the standard self-attention (equation 1). Assuming that the image is split into  $P$  patches, the graph matrices  $G_{k,v,q} \in \mathbb{R}^{P \times P \times d_f}$  and  $G \in \mathbb{R}^{P \times P \times \# \text{heads}}$  are to be chosen for each feature/head from either of the different symmetry preserving graph matrices depicted in Figure 2. The matrix and point-wise multiplication in equation 3 is applied per each feature and head dimension, respectively.

In Figure 2, we highlight variants of a 2D grid topology matrix  $G$  preserving different symmetries, where *same* colors represent a *shared* weight. For example, when using horizontal in 2a, vertices and edges of the same color are transformed into each other, creating a symmetry. Other transformations do not produce this effect. Now, we define  $G$  formally. For more technical details, see Appendix A. Assume that the distances are measured w.r.t. a specific vertex, e.g. the center one in Figure 2, and edges can be viewed as vectors. Then, pick  $G \in \mathbb{R}^{P \times P}$  such that a shared weight is present in  $G$ :

- 2(a). When horizontal component of edges have the same magnitude (Horizontal flip-preserving)
- 2(b). When the magnitude of the edges is same (Horizontal and vertical flip-preserving)
- 2(c). When the distance between vertices is consistent. (Rotation preserving)



(a) Horizontally flip symmetry preserving Graph matrix. Its  $i^{\text{th}}$  column is given by the horizontally flip symmetric graph centered around the  $i^{\text{th}}$  patch vertex (here  $i = 5$ ).

(b) Horizontal and vertical flip preserving graph. Additional rotation symmetry broken by sum over invariance requires green = yellow. (c) Rotation preserving. Flip symmetry broken by sum over directed triangle sub-graphs.

Figure 2. Composition choices of the graph matrix  $G \in \mathbb{R}^{P \times P}$  for  $P = 9$  to preserve different symmetries. Same colours in  $G$  represent shared weights. In (c) flips change the orientation of directed triangles i.e. clockwise to anti-clockwise while  $90^\circ$ -rotations preserve it.

**Flip symmetry breaking layer which preserves rotation symmetry.** To preserve meaning of the direction of the agent (Zhao et al., 2023), it is imperative to break flip-symmetries, as such symmetries interchange the sense of left / right or up / down. To do so, we consider directed triangle sub-graphs. In Figure 2(c), flips and rotation acting are symmetries as they map the graph  $G$  to itself. However, the directed triangle changes orientations from clock-wise to counter-clockwise for flips, while it remains the same for rotations. Applying this insight to the attention score matrix  $\Gamma$  one breaks flip symmetry and preserves the rotation symmetry by summing over distinct directed triangle sub-graphs

$$\begin{aligned} \Gamma^{\text{rot}}(Q, K)_{ij} &= \Theta^{(i \rightarrow j \rightarrow k)} \Gamma(Q, K)_{ij} \\ &+ \Theta^{(j \rightarrow k \rightarrow i)} \Gamma(Q, K)_{jk} + \Theta^{(k \rightarrow i \rightarrow j)} \Gamma(Q, K)_{ki}, \end{aligned} \quad (4)$$

where  $\Theta^{(j \rightarrow k \rightarrow i)}$  are shared weights if the triangle angles are the same; for vertices  $j, k, i$ . The resulting new graph score matrix  $\Gamma^{\text{rot}}$  distinguishes between flips of the input data, but is invariant under  $90^\circ$  left and right rotations.

**Proposition 3.1 (Symmetry Guarantee)** *The GSA mechanism (equation 3) represents a symmetry-preserving module. It may be both invariant and/or equivariant w.r.t. symmetries of the input. The corresponding symmetry is dictated by the various graph selections. To achieve rotation invariance, the subsequent application of equation 4 is necessary. For invariance the token embedding i.e. the artificial  $(P-1)^{\text{th}}$  patch is utilized at the output. Due to this mechanism, self-attention (equation 1) is permutation invariant. **Equivariance** is achieved for the  $P$ -dimensional patch information of the output, i.e. not related to the token embedding.*

**Explicit & Adaptive Symmetry Breaking.** The graph matrices  $G$  and  $G_{k,v,q}$  at weight initialisation explicitly break the symmetry of self-attention from permutation invariance (PI) or equivariance (PE) to the respective choice, see Figure 2. However, PI or PE may be approximately recovered by GSA during training in a self-supervised manner, as

it corresponds simply to the identity matrix  $G, G_{k,v,q} = \mathbf{1}$ . E.g. in Figure 2(b), rotation invariance is obtained if the yellow weights approximate the green ones.

As far as we know, this symmetry-preserving GSA has not appeared previously. Prior work (Fuchs et al., 2020; Romero & Cordonnier, 2021) discuss only modification of the positional embedding. The latter, is entirely omitted by our approach. Symmetries in (Fuchs et al., 2020; Romero & Cordonnier, 2021) are imposed by addition of the positional embedding to the input, however each subsequent attention layer is still PI invariant w.r.t. to its respective inputs. In contrast, in our approach each GSA layer is individually able to reduce PI invariance to graph symmetries and is thus able to infer spatial 2D information of latent features.

## 4. Symmetry-Invariant and Equivariant Transformers

Symmetry invariant transformer (SiT) is a vision transformer that employs the GSA mechanism (equation 3), and optionally equation 4, both locally as well as globally. See Figure 3 for a visualization. We refer to attention applied to entire image patches as “global”. On the other hand, “local” attention is applied to a specific patch or its surrounding neighborhood.

Invariance is obtained by the same mechanism as the permutation-invariance of self-attention, i.e. the token-embedding is added as the  $(P+1)^{\text{th}}$  patch to the input. Since the token embedding does not change under transformations of the input data, the transformer model remains invariant if only the token embedding is considered at the output. In contrast, the representation along the patch dimensions changes under symmetry transformations of the input; however there is a specific way in which one can trace that property throughout the transformer model; we refer to the latter as the equivariant patch-representation. For a more formal argument, please see appendix E.

Based on the above discussion, an invariant SiT forward

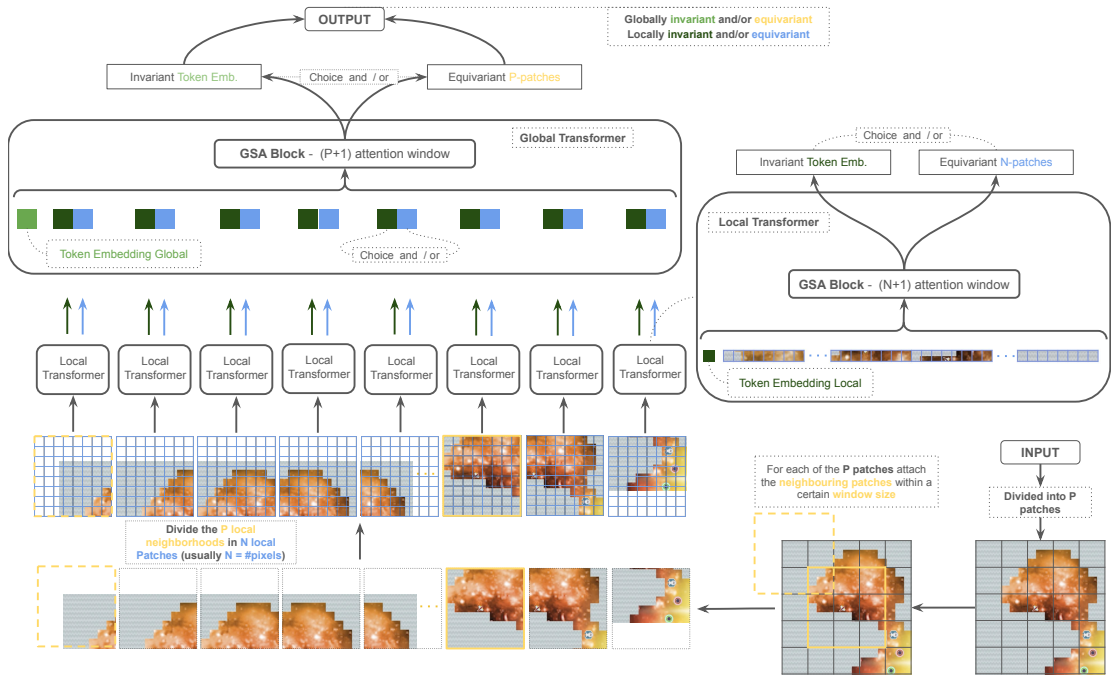


Figure 3. SiT model architecture with local and global GSA modules.

propagates only the symmetry-invariant token embedding to subsequent layers. In contrast, equivariant SiT (**SeT**) forward propagates the equivariant patch-representation both locally and globally. Symmetry-invariant-equivariant Transformer (**SiEts**) is both local and global invariant and equivariant. The global symmetry is a result of the local attention and the global attention mechanism. For example, a global 90° rotation can be thought of as the rotation of the position of the patches (global GSA symmetry) and additionally local rotation of every single patch on pixel level (local GSA symmetry), see Figure 10.

**SiT with Preservation of Directions.** Since all flips alter the interpretation of left/right and up/down, only local and global rotation-invariant SiTs maintain the agent’s meaning of direction. Additionally, Figure 1(c) illustrates that the agent’s surroundings shift with local patch rotations. To address this challenge, we enlarge the local attention window across multiple patches. This "softly" breaks local symmetries, hence, only the global rotation persists as an exact symmetry in our empirically tested invariant SiT version in section 5, the one most fitting for RL tasks. Nonetheless, local symmetries may be restored during training in a self-supervised manner.

**Graph Symmetric Dropout:** A conventional dropout function - likely required for large SiT - models - breaks the inductive bias explicitly. We introduce graph symmetric dropout which preserves the symmetry of SiT. A symmetry preserving dropout for the GSA layer is obtained by setting specific shared weights in the graph matrices  $G$ ,  $G_{k,v,q}$  to zero. This statement follows from proposition 3.1.

### 4.1. Scalability of SiTs

ViTs are known to require more working memory (RAM) of the GPU than CNNs, due to the softmax operation (Dao et al., 2022). The local attention mechanism of SiTs is applied to larger effective batch-sizes as the actual batch-size of the input is compounded by the number of total patches of the global attention. Using a larger local attention window only increases this overflow. In our current implementation, SiTs are 2x-5x times slower to execute than ViTs of comparable size. However, this limitation is due to our custom implementation of our neural-net layers (GSA, graph triangulation) and may be resolved by a future custom CUDA implementation as SiTs can outperform ViTs that contain much larger number of trainable parameters than SiTs.

Nonetheless, technical obstacles arise when scaling SiTs to larger image and batch-sizes in image-based RL environments such as Procgen. We address these by modifying the SiT implementation. First, we establish a connection between graph matrices and depth-wise convolutions with graph-weights as kernels. Secondly, to accommodate for an extended local attention window the graph matrix connects pixels over larger distances while the actual attention-mechanism is focused on a smaller patch.

## 5. Empirical evaluation

### 5.1. Gridworld

**Environment Details.** The LavaCrossing environment is a standard component of MiniGrid, a Minimalistic Gridworld toolkit (Chevalier-Boisvert et al., 2019). The primary

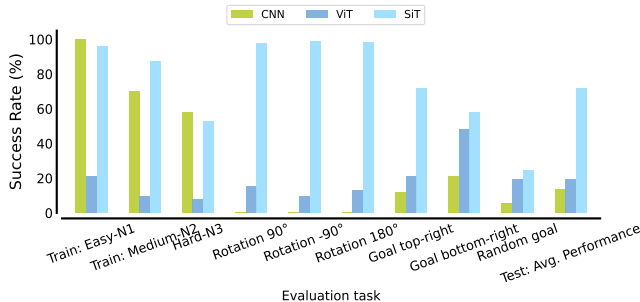


Figure 4. Comparing SiTs with CNNs and ViTs, in terms of training and generalization performance on LavaCrossing environments. SiTs substantially outperform both CNNs and ViTs.

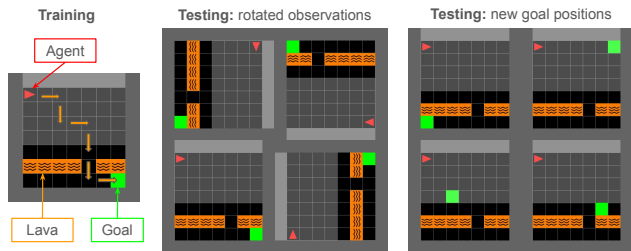


Figure 5. Train vs. test observations of the Mini-grid Lavacrossing (easy-N1) environment. We test generalisation of agents to varying goal and starting positions.

objective of the agent in this environment is to reach the goal position (green square) without falling into the lava river (orange squares). The game is procedurally generated with three levels of difficulty for each map size. Therefore, this environment is suitable for evaluating the combinatorial and out-of-distribution generalization of learned policies in RL. Moreover, we test the generalisation to rotated observations as well as goal changes, see (Figure 5). For further environment details see the appendix F.

**Evaluation & Results.** The experiments with deep Q-learning (IMPALA (Espeholt et al., 2018)) here focuses on GSA with graph matrices  $G_{k,v,q}$ . The number of lava rivers generated in the environment is proportional to the difficulty level. We evaluate the out-of-distribution generalization by training the agent on difficulty level 1 and 2 and testing it on levels 1 to 3, and varying goals unseen during training (Figure 5). As shown in Figure 4, SiTs generalise better than the CNNs even on tasks which do not include rotation symmetry. For an ablation see the appendix G.2.

**5.2. Scaling SiTs: Progen, Atari 100k & DM-control**

We demonstrate scalability of SiTs in the widely-studied Progen benchmark (Cobbe et al., 2020), Atari 100k (Belle-mare et al., 2013; Kaiser et al., 2020) and DM-control (Tassa et al., 2018). For details of the latter see the appendix F.4 and F.3, respectively. The Progen benchmark corresponds

to a distribution of partially observable MDPs (POMDPs)  $q(m)$ , and each level of a game corresponds to a POMDP sampled from that game’s distribution  $m \sim q$ . The POMDP  $m$  is determined by the random seed used to generate the corresponding level. Following the setup from (Cobbe et al., 2020), agents are trained on a fixed set of  $n = 200$  levels (generated using seeds from 1 to 200) and tested on the full distribution of levels (generated by sampling seeds uniformly at random from all computer integers). We evaluate test performance on 20 different levels.

Table 1 shows the results for SiT, the equivariant SeT as well as a both invariant & equivariant SieT trained with PPO (DrAC (Raileanu et al., 2020)) with crop-data augmentation. SiT\* uses two consecutive sums over triangles of the attention score matrix. Invariant SiTs perform well in environments not reflecting the symmetries of the model, e.g. Starpilot, Fruitbot, Chaser are not rotation invariant. However, the combination of invariance and equivariance of SieTs is superior.

**Results:** SiT almost doubles the performance on the rotation invariant Caveflyer environment w.r.t. to the ResNet (620k weights) of UCB-DrAC (Raileanu et al., 2020). As UCB-Drac uses the rotational data-augmentation for training, we can conclude that SiTs outperform rotational data-augmentation. Overall, our tested SiTs, SeT and SieT models ( $\approx 70k$  weights) substantially outperform the CNN and E2CNN (4-layers) (Weiler & Cesa, 2021) baselines with similar number of weights while perform comparably to the UCB-ResNet with  $9\times$  parameters (620k weights). Notably, all the SiT variants obtain  $7 - 9\times$  improvements in performance compared to ViTs.

**Proof-of-concept Atari 100k and DM-control:** We evaluate our SieT model on 5 common Atari games, SpaceInvaders, Pong, Breakout, KungFuMaster, MsPacman, and find comparable sample-efficiency to the baseline CNN (Hessel et al., 2017; Micheli et al., 2023), see Figures 12 and 13 and Table 3. We also test 1D shift-symmetric GSA in the transformer world-model (Micheli et al., 2023), see Figure 11. DM-control: We employ SieT on top of SAC (Haarnoja et al., 2018) on the Walker-walk task. Without any hyper-parameter and backbone changes compared to our Progen setup, SieT has comparable performance to the ViT baseline with  $> 1M$  weights (Hansen & Wang, 2021).

**Hyperparameter Sensitivity .** The same limited h-parameter search was performed for SiTs and ViTs. Compared to the ResNet baseline (Raileanu et al., 2020), we employ larger batch-size 96 (instead 8) and PPO-epoch of 2 (instead 3). SiTs don’t require tuning except for the batch-size, e.g., a PPO-epoch of 3 works well too. No tuning at all on DM-control and Atari 100k. ViTs generally exhibit suboptimal performance in RL, with the notable exception of (Hansen et al., 2021; Tang & Ha, 2021). We attribute

Procgen Task	CNN	E2CNN	E2CNN'	ViT	SiT	SiT*	SeT	SieT	CNN-UCB* (9×)
CaveFlyer	4.0%	13.4%	17.7%	-1.8%	<b>59.7%</b>	<b>55.5%</b>	4.6%	<b>34.5%</b>	18.0%
StarPilot	36.3%	28.1%	29.4%	6.7%	31.3%	31.0%	38.4%	<b>42.2%</b>	44.6%
Fruitbot	70.8%	64.0%	66.1%	9.7%	69.8%	70.5%	68.9%	<b>76.0%</b>	85.8%
Chaser	10.6%	13.6%	15.6%	9.0%	35.6%	45.6%	50.1%	<b>54.0%</b>	44.6%
Average	30.4%	29.8 %	32.2 %	5.9 %	49.1 %	<b>50.6 %</b>	40.5 %	<b>51.7 %</b>	48.2%

Table 1. CNN/ViT vs. SiTs on Procgen environments: Caveflyer, Starpilot, Chaser, Fruitbot. We train with PPO (DrAC) + Crop augmentation for SiT (SiT\*, SeT, SieT) and compare to the CNN, and E2CNN with Dihedral symmetry group (Wang et al., 2022a) (ResNet with model size 79.4k comparable to the SiT - 65.7k; ViT with 4-layers - 216k, E2CNN with 4-layers 70.7k, and E2CNN' with 4-layers 139.2k (increased features) ). We do not alter the ResNet architecture of (Raileanu et al., 2020) but chose the same hidden-size of 64 as for the SiT as well reduce the number of channels to [4,8,16]. We train over 25M steps. Following Agarwal et al. (2021b), we report the min-max normalized score that shows how far we are from maximum achievable performance on each environment. All scores are computed by averaging over both the 4 seeds and over the 23M-25M test-steps. The UCB-DrAC results with Impala-CNN(×4) ResNet with 620k parameters are taken from (Raileanu et al., 2020).

this that ViTs are less sample-efficient and require different hyperparameter compared to CNNs. As Vits are compute extensive hyperparameter search is practically infeasible. **SiTs are applicable to RL tasks as they alleviate both of these caveats.**

**Latent representation analysis:** In Figure 6, we present a principal component analysis (PCA) of the latent representation of the policy SiT model. While local symmetries and global flips have been **dynamically broken** during training exact symmetries of **global rotation is preserved**, i.e. all the data-points collapse into (nearly) identical points for the latter. As by design of SiTs, the local attention patch symmetry - *local center rot.* in Figure 6 - is broken "softly" as it is relatively close to the original latent representation. Note that at weight initialisation of SiT, all of the symmetries except permutation invariance are almost exactly preserved.

### 5.3. SiTs beyond RL: Vision Task Ablation

We perform an ablation study of SiTs, SieTs compared to ViTs on a supervised vision task on the CIFAR-10 dataset (Krizhevsky & Hinton, 2009) see Figure 2b; firstly we compare  $G$  in SiT to a conventional position embedding in ViT; secondly we use our SieT model with  $G_{k,q}, G_v, G = 1$  to show improved sample efficiency & performance compared to ViTs (Dosovitskiy et al., 2020). SiT and SieT use the horizontal flip symmetry preserving graph matrices.

**Results.** The permutation invariance in ViTs is broken by the use of a positional embedding; in SiTs by the graph matrix  $G$  in Equation (3). While removing positional embedding to obtain local and global permutation invariance substantially degrades performance (56% test accuracy), using our graph symmetric attention (80% test accuracy) is superior to using positional embedding globally (76% test accuracy). Furthermore, Figure 7b shows that SiTs and SieTs reach same performance as ViTs but using 2 – 5× less training epochs. We perform extensive ablations studies on the impact of patch-size changes of SiTs on CIFAR 10

in appendix H.

### 5.4. Entire Procgen Suite SieT

In this section we evaluate a smaller SieT variant (41k weights) on the entirety of the Procgen suite of 16 games, see Figure (8). We conclude that SieT outperforms a comparable CNN on average over the 16 games. The lower total score compared to Table (1) is due to two main factors. First, both the tiny SieT and CNN variant do not perform on several environments in combination with DrAC. Second, the game selection in Table (1) reflects a collection of very successful environments of DrAC.

### 5.5. Limitations of SiTs

Equivariant CNN based networks (Wang et al., 2022a) have shown promise in particular in environments which admit symmetry but also where latent dynamics admit symmetries (Wang et al., 2023). At the core we provide a Transformer based alternative which outperforms E2CNN for comparable model sizes see Table (1). Thus in general SiT will offer benefits over CNNs in environments where at least some remnant symmetries other than shift symmetries are present - this is in accordance with our findings. Additionally, we observed benefits of SiTs in terms of their generalization performance due to unseen tasks, while performance in single-task RL on the same training and test task settings seem to be comparable to CNNs. It is worth noting that except for the Caveflyer environment, other environments in ProcGen do not admit strong symmetry properties, which would favor SiTs over CNNs off the shelf.

From our ablation studies on Minigrid see appendix Table (5) we conclude that local GSA is of significant importance to get the performance benefits. However, as we discuss in section 4.1 "Scalability of SiT" the local GSA layer poses compute and memory challenges for application to larger model sizes and complex tasks.

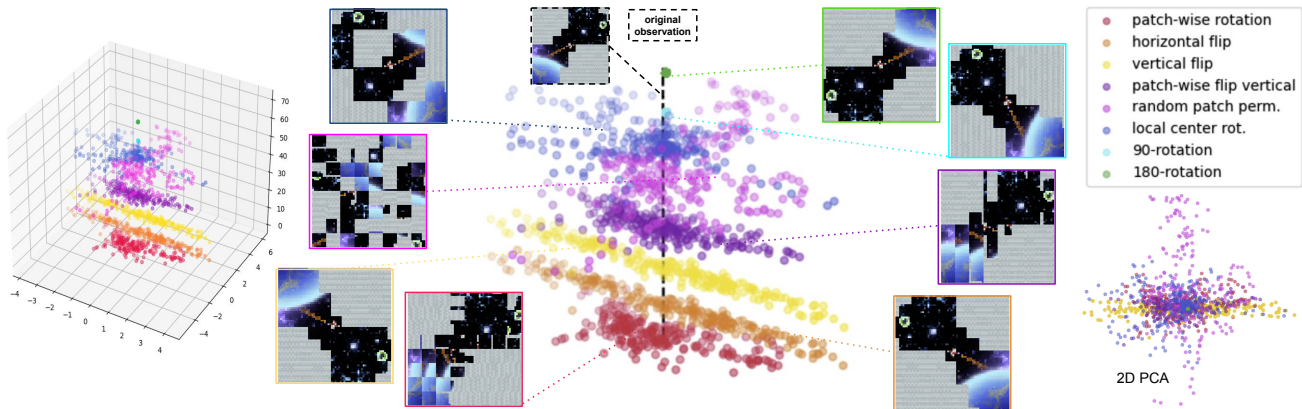
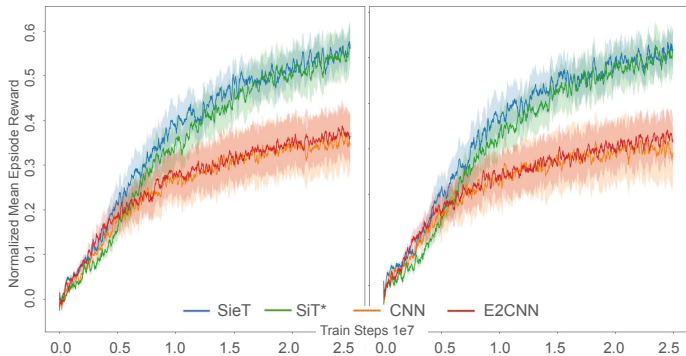
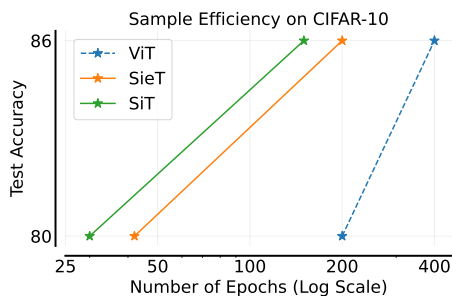


Figure 6. PCA of latent space representation of the trained SiT model after 25M steps on Procgen CaveFlyer. We display the PCA of the difference of the latent representation of augmented observations and original ones. 3D-view (left and center) - vertical separation for illustration purposes - 2D-view i.e. from above (bottom-right).



(a) Train (left) and test curves (right), normalized reward averaged over the StarPilot, CaveFlyer, Chaser, Fruitbot environments.



(b) SiTs and SieTs are much more sample efficient than ViTs (Dosovitskiy et al., 2020). The SieT model has 4 local GSA layers and 8 global ones.

Figure 7. SiTs are comparable to CNNs in terms of sample efficiency on Procgen (a) and outperform conventional ViTs (b).

Let us stress that we have evaluated SiTs (and SieTs) on a large variety of tasks, namely Minigrid, Procgen, Atari, DM-control, and CIFAR10. The major limitation to SiTs currently are the compute and memory expenses that arise in the SiT architecture from the local GSA. With increased computational cost for each **local GSA** layer added. The latter, trade-offs for improved sample-efficiency see Figure (7b). Our work serves as a proof-of-concept for the approach and work while more efficient future custom implementation of SiTs may alleviate some of the computational cost.

One specific example of failure is Procgen in the new rebuttal study see section 5.4 is that both the SieT and CNN variant do not learn the BossFight task very well. However, on the CNN side when adding more convolutional layers adequately the model starts to learn well.

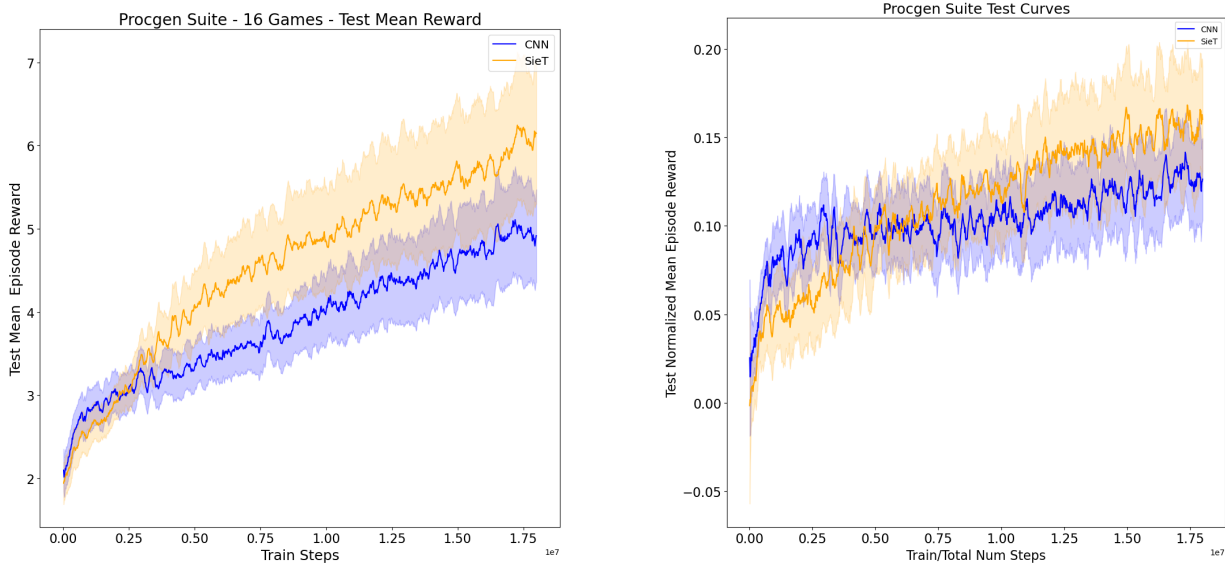
## 6. Related Work

Symmetry is a prevalent implicit approach in deep learning for designing neural networks with established equiv-

ariances and invariances. The literature on symmetries in Vision Transformers (ViTs) (Fuchs et al., 2020; Romero & Cordonnier, 2021) is relatively limited compared to CNNs (LeCun et al., 1989; Zhang, 1990; Zhang & Sejnowski, 1988), recurrent neural networks (Hochreiter & Schmidhuber, 1997; Rumelhart et al., 1986), graph neural networks (Maron et al., 2019; Satorras et al., 2021a), and capsule networks (Sabour et al., 2017). PI in attention mechanisms and ViTs has been examined in (Lee et al., 2019) and (Tang & Ha, 2021). In contrast, the SiT variants admit different adaptive symmetries other than PI.

The Region ViT method (Chen et al., 2022) divides the feature map into local areas, where each region has tokens that attend to their local counterparts. We use global tokens and use local attention in a neighbouring subset. The method in (Wang et al., 2021) combines local and global attention to reduce complexity, focusing globally on specific windows. For us "global" means standard attention, while "local" pertains to attention within a window.





(a) Mean episode test reward averaged over 16 games, and 4 seeds, respectively.

(b) Normalized mean episode test reward averaged over 16 games, and 4 seeds, respectively.

Figure 8. Empirical evaluation on entire Procgen suite i.e the reward is averaged over 16 games and standard error of SieT model (41k weights) and a CNN (40k weights) on top of DrAC with crop augmentation over 18M training steps. The CNN consist of 4 convolutions layers with channel dimensions [4, 8, 16, 32], respectively. The SieT model contains two local GSA layers with features [16, 32], and to global ones with 64 features, respectively. both the CNN and SieT policy have a hidden-size of 64.

Conventionally sample efficiency is enhanced by data augmentation (Krizhevsky et al., 2012). Simple image augmentations, such as random crop (Laskin et al., 2020) or shift (Yarats et al., 2021a), can improve RL generalisation performance; in particular when combined with contrastive learning (Agarwal et al., 2021a). SiTs are complementary to data-augmentation.

Algebraic symmetries in Markov Decision Processes (MDP) were initially discussed in (Balaraman & Andrew, 2004) and recently contextualized within RL in (van der Pol et al., 2020). Symmetry-based representation learning (Higgins et al., 2018) refers to the study of symmetries of the environment manifested in the latent representation and was extended to environmental interactions in (Caselles-Dupré et al., 2019). These concepts were recently extended in (Mondal et al., 2022; Rezaei-Shoshtari et al., 2022). In (Weissenbacher et al., 2022), symmetries of the dynamics are inferred in a self-supervised manner; (Cheng et al., 2023) discusses time-reversal symmetry. These approaches are mostly complimentary to employing SiTs with equivariance/invariance which may aid the former.

Numerous prior works have demonstrated the exceptional sample efficiency of RL achieved through equivariant methods with CNNs (van der Pol & Welling, 2019; Wang & Walters, 2022). Steerable Equivariant CNNs named E2CNNs (Cohen & Welling, 2016; Weiler & Cesa, 2021) have been widely applied to RL (Mondal et al., 2020; Wang et al.,

2022a). In contrast, SiTs belong to ViT paradigm, i.e. a distinct new approach to achieve invariance as well as equivariance both locally and globally. Approximately equivariant networks (Wang et al., 2022b) offer a flexible and adaptive approach by imposing constraints on the weights via a regularizer. Rotation invariance steerable convolution in toy-examples is discussed in (Zhao et al., 2023). SiTs start from a manifest PI and describe an implicit adaptive mechanism of breaking it and scale to relevant tasks in RL.

## 7. Conclusions

In this work, we introduced the Graph Symmetric Attention (GSA) mechanism, a symmetry-preserving attention layer that adapts the self-attention mechanism to maintain graph symmetries. We combine GSA with ViTs to propose the novel SiT architecture. By leveraging the interplay of local and global information, SiT achieves inherent out-of-distribution generalization on RL environments.

Transformers have significantly advanced natural-language-processing and vision tasks, particularly in scalability. Our work may pave the way for applying these benefits to image-based RL. Additionally, transformers facilitate integration with Large Language Models (LLMs) for multimodal architectures, highlighting their potential in future vision and language-based RL research.

## Impact Statement

This paper presents work whose goal is to advance the field of Machine Learning. There are many potential societal consequences of our work, none which we feel must be specifically highlighted here.

## Acknowledgments

We would like express our gratitude to Yujin Tang for helpful comments on the draft. And, we would like to thank Y. Nishimura for technical support. This work was supported by JSPS KAKENHI (Grant Number JP22H00516), and JST CREST (Grant Number JPMJCR1913).

## References

- Agarwal, R., Machado, M. C., Castro, P. S., and Bellemare, M. G. Contrastive behavioral similarity embeddings for generalization in reinforcement learning. *arXiv preprint arXiv:2101.05265*, 2021a.
- Agarwal, R., Schwarzer, M., Castro, P. S., Courville, A. C., and Bellemare, M. Deep reinforcement learning at the edge of the statistical precipice. *Advances in neural information processing systems*, 34:29304–29320, 2021b.
- Balaraman, R. and Andrew, G. B. Approximate homomorphisms: A framework for non-exact minimization in markov decision processes. In *In International Conference on Knowledge Based Computer Systems*, 2004.
- Battaglia, P. W., Hamrick, J. B., Bapst, V., Sanchez-Gonzalez, A., Zambaldi, V. F., Malinowski, M., Tacchetti, A., Raposo, D., Santoro, A., Faulkner, R., Çaglar Gülçehre, Song, H. F., Ballard, A. J., Gilmer, J., Dahl, G. E., Vaswani, A., Allen, K. R., Nash, C., Langston, V., Dyer, C., Heess, N., Wierstra, D., Kohli, P., Botvinick, M., Vinyals, O., Li, Y., and Pascanu, R. Relational inductive biases, deep learning, and graph networks. *CoRR*, abs/1806.01261, 2018. URL <http://arxiv.org/abs/1806.01261>.
- Bellemare, M., Veness, J., and Bowling, M. Investigating contingency awareness using atari 2600 games. In *Proceedings of the AAAI Conference on Artificial Intelligence*, volume 26, pp. 864–871, 2012.
- Bellemare, M. G., Naddaf, Y., Veness, J., and Bowling, M. The arcade learning environment: An evaluation platform for general agents. *Journal of Artificial Intelligence Research*, 47:253–279, jun 2013.
- Bellemare, M. G., Candido, S., Castro, P. S., Gong, J., Machado, M. C., Moitra, S., Ponda, S. S., and Wang, Z. Autonomous navigation of stratospheric balloons using reinforcement learning. *Nature*, 588(7836):77–82, 2020.
- Beyer, L., Zhai, X., and Kolesnikov, A. Better plain vit baselines for imagenet-1k, 2022.
- Beyer, L., Izmailov, P., Kolesnikov, A., Caron, M., Kornblith, S., Zhai, X., Minderer, M., Tschannen, M., Alabdulmohsin, I., and Pavetic, F. Flexivit: One model for all patch sizes, 2023.
- Caselles-Dupré, H., Garcia Ortiz, M., and Filliat, D. Symmetry-based disentangled representation learning requires interaction with environments. In Wallach, H., Larochelle, H., Beygelzimer, A., d'Alché-Buc, F., Fox, E., and Garnett, R. (eds.), *Advances in Neural Information Processing Systems*, volume 32. Curran Associates, Inc., 2019.
- Chen, C.-F., Panda, R., and Fan, Q. Regionvit: Regional-to-local attention for vision transformers, 2022.
- Chen, L., Lu, K., Rajeswaran, A., Lee, K., Grover, A., Laskin, M., Abbeel, P., Srinivas, A., and Mordatch, I. Decision transformer: Reinforcement learning via sequence modeling, 2021.
- Cheng, P., Zhan, X., Wu, Z., Zhang, W., Song, S., Wang, H., Lin, Y., and Jiang, L. Look beneath the surface: Exploiting fundamental symmetry for sample-efficient offline rl, 2023.
- Chevalier-Boisvert, M., Bahdanau, D., Lahlou, S., Willems, L., Saharia, C., Nguyen, T. H., and LeBret, R. Babyai: First steps towards grounded language learning with a human in the loop. *International Conference on Learning Representations*, 2019.
- Cobbe, K., Hesse, C., Hilton, J., and Schulman, J. Leveraging procedural generation to benchmark reinforcement learning. In III, H. D. and Singh, A. (eds.), *Proceedings of the 37th International Conference on Machine Learning*, volume 119 of *Proceedings of Machine Learning Research*, pp. 2048–2056. PMLR, 13–18 Jul 2020.
- Cohen, T. and Welling, M. Group equivariant convolutional networks. In Balcan, M. F. and Weinberger, K. Q. (eds.), *Proceedings of The 33rd International Conference on Machine Learning*, volume 48 of *Proceedings of Machine Learning Research*, pp. 2990–2999, New York, New York, USA, 20–22 Jun 2016. PMLR.
- Dao, T., Fu, D. Y., Ermon, S., Rudra, A., and Ré, C. FlashAttention: Fast and memory-efficient exact attention with IO-awareness. In *Advances in Neural Information Processing Systems*, 2022.
- Dosovitskiy, A., Beyer, L., Kolesnikov, A., Weissenborn, D., Zhai, X., Unterthiner, T., Dehghani, M., Minderer, M., Heigold, G., Gelly, S., Uszkoreit, J., and Houlsby, N. An image is worth 16x16 words: Transformers for image recognition at scale, 2020.

- Espeholt, L., Soyer, H., Munos, R., Simonyan, K., Mnih, V., Ward, T., Doron, Y., Firoiu, V., Harley, T., Dunning, I., et al. Impala: Scalable distributed deep-rl with importance weighted actor-learner architectures. *arXiv preprint arXiv:1802.01561*, 2018.
- Fuchs, F., Worrall, D., Fischer, V., and Welling, M. Se(3)-transformers: 3d roto-translation equivariant attention networks. In Larochelle, H., Ranzato, M., Hadsell, R., Balcan, M., and Lin, H. (eds.), *Advances in Neural Information Processing Systems*, volume 33, pp. 1970–1981. Curran Associates, Inc., 2020. URL [https://proceedings.neurips.cc/paper\\_files/paper/2020/file/15231a7ce4ba789d13b722cc5c955834-Paper.pdf](https://proceedings.neurips.cc/paper_files/paper/2020/file/15231a7ce4ba789d13b722cc5c955834-Paper.pdf).
- Haarnoja, T., Zhou, A., Abbeel, P., and Levine, S. Soft actor-critic: Off-policy maximum entropy deep reinforcement learning with a stochastic actor. In Dy, J. and Krause, A. (eds.), *Proceedings of the 35th International Conference on Machine Learning*, volume 80 of *Proceedings of Machine Learning Research*, pp. 1861–1870. PMLR, 10–15 Jul 2018.
- Hansen, N. and Wang, X. Generalization in reinforcement learning by soft data augmentation. In *International Conference on Robotics and Automation*, 2021.
- Hansen, N., Su, H., and Wang, X. Stabilizing deep q-learning with convnets and vision transformers under data augmentation. *Advances in neural information processing systems*, 34:3680–3693, 2021.
- Hassani, A., Walton, S., Shah, N., Abuduweili, A., Li, J., and Shi, H. Escaping the big data paradigm with compact transformers, 2022.
- Hessel, M., Modayil, J., van Hasselt, H., Schaul, T., Ostrovski, G., Dabney, W., Horgan, D., Piot, B., Azar, M., and Silver, D. Rainbow: Combining improvements in deep reinforcement learning, 2017.
- Higgins, I., Amos, D., Pfau, D., Racaniere, S., Matthey, L., Rezende, D., and Lerchner, A. Towards a definition of disentangled representations, 2018.
- Hochreiter, S. and Schmidhuber, J. Long short-term memory. *Neural computation*, 9(8):1735–1780, 1997.
- Jiang, Z., Minervin, P., Jiang, M., and Rocktäschel, T. Grid-to-graph: Flexible spatial relational inductive biases for reinforcement learning. In *AAMAS 2021*, 2021.
- Kaiser, L., Babaeizadeh, M., Milos, P., Osinski, B., Campbell, R. H., Czechowski, K., Erhan, D., Finn, C., Koza-kowski, P., Levine, S., et al. Model-based reinforcement learning for atari. In *International Conference on Learning Representations*, 2020.
- Kitano, H., Asada, M., Kuniyoshi, Y., Noda, I., and Osawa, E. Robocup: A challenge problem for ai and robotics. In *RoboCup-97: Robot soccer world cup I*, pp. 1–19. Springer, 1997.
- Krizhevsky, A. and Hinton, G. Learning multiple layers of features from tiny images. Technical report, Citeseer, 2009.
- Krizhevsky, A., Sutskever, I., and Hinton, G. E. Imagenet classification with deep convolutional neural networks. In *Advances in Neural Information Processing Systems*, pp. 1097–1105, 2012.
- Küttler, H., Nardelli, N., Lavril, T., Selvatici, M., Sivakumar, V., Rocktäschel, T., and Grefenstette, E. TorchBeast: A PyTorch Platform for Distributed RL. *arXiv preprint arXiv:1910.03552*, 2019. URL <https://github.com/facebookresearch/torchbeast>.
- Laskin, M., Lee, K., Stooke, A., Pinto, L., Abbeel, P., and Srinivas, A. Reinforcement learning with augmented data. In Larochelle, H., Ranzato, M., Hadsell, R., Balcan, M., and Lin, H. (eds.), *Advances in Neural Information Processing Systems*, volume 33, pp. 19884–19895. Curran Associates, Inc., 2020. URL <https://proceedings.neurips.cc/paper/2020/file/e615c82aba461681ade82da2da38004a-Paper.pdf>.
- LeCun, Y., Boser, B. E., Denker, J. S., Henderson, D., Howard, R. E., Hubbard, W., and Jackel, L. D. Back-propagation applied to handwritten zip code recognition. *Neural computation*, 1(4):541–551, 1989.
- Lee, J., Lee, Y., Kim, J., Kosiorek, A., Choi, S., and Teh, Y. W. Set transformer: A framework for attention-based permutation-invariant neural networks. In *Proceedings of the 36th International Conference on Machine Learning*. PMLR, 2019. URL <https://proceedings.mlr.press/v97/lee19d.html>.
- Maron, H., Ben-Hamu, H., Shamir, N., and Lipman, Y. Invariant and equivariant graph networks. In *International Conference on Learning Representations*, 2019.
- Micheli, V., Alonso, E., and Fleuret, F. Transformers are sample-efficient world models. In *The Eleventh International Conference on Learning Representations*, 2023. URL <https://openreview.net/forum?id=vhFulAcb0xb>.
- Mondal, A. K., Nair, P., and Siddiqi, K. Group equivariant deep reinforcement learning, 2020.

- Mondal, A. K., Jain, V., Siddiqi, K., and Ravanbakhsh, S. EqR: Equivariant representations for data-efficient reinforcement learning. In Chaudhuri, K., Jegelka, S., Song, L., Szepesvari, C., Niu, G., and Sabato, S. (eds.), *Proceedings of the 39th International Conference on Machine Learning*, volume 162 of *Proceedings of Machine Learning Research*, pp. 15908–15926. PMLR, 17–23 Jul 2022.
- Raileanu, R., Goldstein, M., Yarats, D., Kostrikov, I., and Fergus, R. Automatic data augmentation for generalization in deep reinforcement learning. *arXiv preprint arXiv:2006.12862*, 2020.
- Rezaei-Shoshtari, S., Zhao, R., Panangaden, P., Meger, D., and Precup, D. Continuous mdp homomorphisms and homomorphic policy gradient, 2022.
- Romero, D. W. and Cordonnier, J.-B. Group equivariant stand-alone self-attention for vision. In *International Conference on Learning Representations*, 2021. URL <https://openreview.net/forum?id=JkfYjnOEo6M>.
- Rumelhart, D. E., Hinton, G. E., and Williams, R. J. Learning representations by back-propagating errors. *Nature*, 323(6088):533–536, 1986.
- Sabour, S., Frosst, N., and Hinton, G. E. Dynamic routing between capsules. In *Advances in Neural Information Processing Systems*, pp. 3856–3866, 2017.
- Satorras, V. G., Hoogeboom, E., and Welling, M. E(n)-equivariant graph neural networks. In *International Conference on Learning Representations*, 2021a.
- Satorras, V. G., Hoogeboom, E., and Welling, M. E(n) equivariant graph neural networks. *arXiv preprint arXiv:2102.09844*, 2021b.
- Schrittwieser, J., Antonoglou, I., Hubert, T., Simonyan, K., Sifre, L., Schmitt, S., Guez, A., Lockhart, E., Hassabis, D., Graepel, T., et al. Mastering atari, go, chess and shogi by planning with a learned model. *Nature*, 588(7839): 604–609, 2020.
- Silver, D., Huang, A., Maddison, C. J., Guez, A., Sifre, L., van den Driessche, G., Schrittwieser, J., Antonoglou, I., Panneershelvam, V., Lanctot, M., et al. Mastering the game of go with deep neural networks and tree search. *nature*, 529(7587):484–489, 2016.
- Su, J., Lu, Y., Pan, S., Wen, B., and Liu, Y. Roformer: Enhanced transformer with rotary position embedding. *CoRR*, abs/2104.09864, 2021. URL <https://arxiv.org/abs/2104.09864>.
- Tang, Y. and Ha, D. The sensory neuron as a transformer: Permutation-invariant neural networks for reinforcement learning. In Beygelzimer, A., Dauphin, Y., Liang, P., and Vaughan, J. W. (eds.), *Advances in Neural Information Processing Systems*, 2021. URL <https://openreview.net/forum?id=wtLW-Amuds>.
- Tassa, Y., Doron, Y., Muldal, A., Erez, T., Li, Y., de Las Casas, D., Budden, D., Abdolmaleki, A., Merel, J., Lefrancq, A., Lillicrap, T. P., and Riedmiller, M. A. Deepmind control suite. *CoRR*, abs/1801.00690, 2018. URL <http://arxiv.org/abs/1801.00690>.
- van der Pol, E. and Welling, M. On the benefits of invariance in neural networks. In *International Conference on Learning Representations*, 2019.
- Van der Pol, E., Worrall, D., van Hoof, H., Oliehoek, F., and Welling, M. Mdp homomorphic networks: Group symmetries in reinforcement learning. *Advances in Neural Information Processing Systems*, 33:4199–4210, 2020.
- van der Pol, E., Worrall, D., van Hoof, H., Oliehoek, F., and Welling, M. Mdp homomorphic networks: Group symmetries in reinforcement learning. In Larochelle, H., Ranzato, M., Hadsell, R., Balcan, M. F., and Lin, H. (eds.), *Advances in Neural Information Processing Systems*, volume 33, pp. 4199–4210. Curran Associates, Inc., 2020.
- Veličković, P., Cucurull, G., Casanova, A., Romero, A., Liò, P., and Bengio, Y. Graph attention networks. In *International Conference on Learning Representations*, 2018. URL <https://openreview.net/forum?id=rJXMpikCZ>.
- Wang, D. and Walters, R. So (2) equivariant reinforcement learning. In *International Conference on Learning Representations*, 2022.
- Wang, D., Walters, R., and Platt, R.  $\mathrm{SO}(2)$ -equivariant reinforcement learning. In *International Conference on Learning Representations*, 2022a. URL [https://openreview.net/forum?id=7F9cOhdvmfk\\_](https://openreview.net/forum?id=7F9cOhdvmfk_).
- Wang, D., Park, J. Y., Sortur, N., Wong, L. L., Walters, R., and Platt, R. The surprising effectiveness of equivariant models in domains with latent symmetry. In *The Eleventh International Conference on Learning Representations*, 2023. URL <https://openreview.net/forum?id=P4MUGRM4Acu>.
- Wang, R., Walters, R., and Yu, R. Approximately equivariant networks for imperfectly symmetric dynamics. In Chaudhuri, K., Jegelka, S., Song, L., Szepesvari, C., Niu, G., and Sabato, S. (eds.), *Proceedings of the 39th International Conference on Machine Learning*, volume 162

of *Proceedings of Machine Learning Research*. PMLR, 2022b.

Wang, W., Yao, L., Chen, L., Lin, B., Cai, D., He, X., and Liu, W. Crossformer: A versatile vision transformer hinging on cross-scale attention, 2021.

Weiler, M. and Cesa, G. General  $e(2)$ -equivariant steerable cnns, 2021.

Weissenbacher, M., Sinha, S., Garg, A., and Kawahara, Y. Koopman q-learning: Offline reinforcement learning via symmetries of dynamics. In *International Conference on Machine Learning*, pp. 23645–23667. PMLR, 2022.

Yarats, D., Kostrikov, I., and Fergus, R. Data-efficient reinforcement learning with momentum predictive representations. In *International Conference on Learning Representations*, 2021a.

Yarats, D., Kostrikov, I., and Fergus, R. Image augmentation is all you need: Regularizing deep reinforcement learning from pixels. In *International Conference on Learning Representations*, 2021b. URL <https://openreview.net/forum?id=GY6-6sTvGaf>.

Ye, D., Liu, S., Tian, Y., and Liu, Q. Mastering atari games with limited data. In *Advances in Neural Information Processing Systems*, volume 34, 2021.

Zhang, K. Interpreting the internal vector representation of an analogical neural network. In *Proceedings of the 12th annual conference of the Cognitive Science Society*, pp. 684–691. Lawrence Erlbaum Associates, 1990.

Zhang, K. and Sejnowski, T. J. Parallel distributed processing: Explorations in the microstructure of cognition, vol. 1. In *Foundations*. MIT Press, 1988.

Zhao, L., Zhu, X., Kong, L., Walters, R., and Wong, L. L. Integrating symmetry into differentiable planning with steerable convolutions. In *The Eleventh International Conference on Learning Representations*, 2023. URL <https://openreview.net/forum?id=n7CPzMPKQ1>.

## A. Overview of Definitions: Graph Symmetric Attention Mechanism

We propose the following Graph Symmetric Attention (GSA) mechanism in equation 11. Where  $G, G_{k,v,q}, G_{kq,b} \in \mathbb{R}^{P \times P}$  being the graph matrices described in figure 2 and  $\sigma$  is an activation function. The color coding refers to different conceptual implementations, which may be used in combination. When using token embeddings  $K, V, Q, \in \mathbb{R}^{P+1 \times d_f}$  thus  $G_{k,v,q} \in \mathbb{R}^{P+1 \times P+1 \times d_f}$  and  $G, G_{kq,b} \in \mathbb{R}^{P+1 \times P+1 \times \#heads}$ . In particular, that implies that we apply a different set of graph weights to the feature and head dimensions. See Figure (9) for a visualisation.

Moreover, we propose the a second variant of the GSA<sup>a-sym</sup> of our attention mechanism which replaces the attention matrix as

$$\begin{aligned} & \text{softmax}\left(\frac{1}{\sqrt{d_q}} \text{sym}(\Gamma(Q, K))\right) \\ & + \text{softmax}\left(\frac{1}{\sqrt{d_q}} \text{a-sym}(\Gamma(Q, K))\right) \end{aligned} \quad (6)$$

where we symmetrise and anti-symmetrises over the patch indices of  $\Gamma(Q, K)$  respectively, the latter is as in equation 3; and *a-sym* refers to replacing the symmetrisation in equation 11 by anti-symmetrisation. Anti-symmetrisation of a matrix M refers to  $M_{ij} \rightarrow M_{ij} - M_{ji}$ .

### Empirical Evaluation Omission Overview:

- On our grid-world environment experiments we found qualitatively that the variants  $G_{kq,b}, G$  required more h-parameter tuning to show comparable performance to the CNN baseline. We thus removed a quantitative analysis from the paper.<sup>2</sup>
- Adding the anti-symmetrisation equation 6 to the architecture increased generalisation performance on the grid-world environment. However, it requires two softmax operation, which renders it hard to scale; we thus removed a quantitative analysis from the paper.

**More formally of can define e.g. G in Figure 2 (c).** Pick  $G \in \mathbb{R}^{P \times P}$  such that it admits a shared weight if the distance between vertices is the same. For more technical details see the appendix A More formally,  $G_{ij} = \theta^{(\kappa)}, i, j = 1, \dots, P$  with weights  $\theta$  with labels  $\kappa = 1, \dots, \#(\text{unique edge lengths of 2D grid graph})$ . The element  $G_{ij}$  corresponds to the edge between the  $i^{\text{th}}$  and  $j^{\text{th}}$  vertex, i.e. the assigned weight index  $\kappa$  is identical if and

<sup>2</sup>Let us stress that both  $G$  and  $G_{v,k,q}$  are indeed sufficient to break symmetries, respectively, i.e. to achieve the desired equivariance.

## SiT: Symmetry-Invariant Transformers for Generalisation in RL

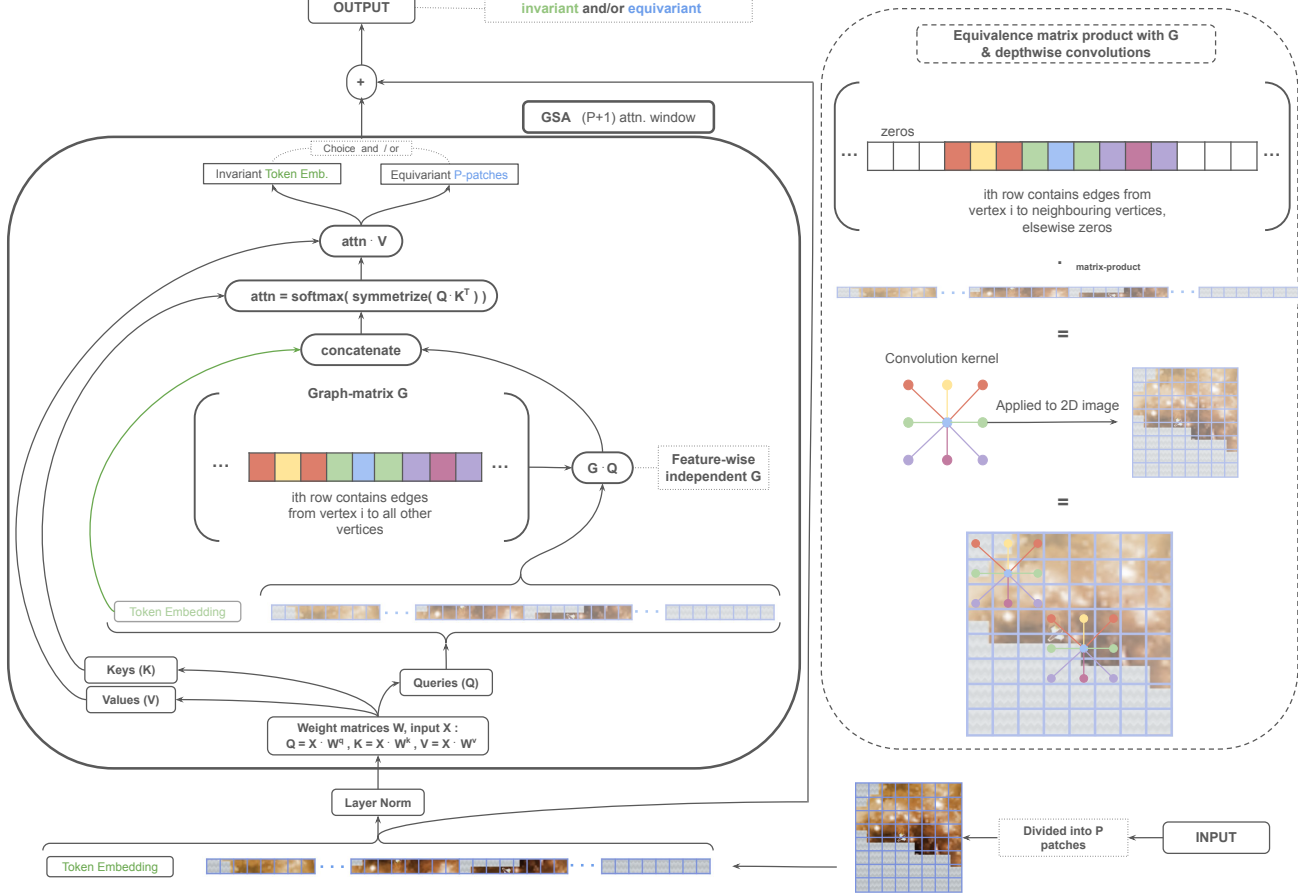


Figure 9. GSA module architecture (left), and equivalence of graph matrix and depth-wise convolutions (right). The GSA layer includes Layer-Norm and additive skip connection in addition to the GSA module. We display the GSA variant  $G_{k,v,q}$  with  $G_{k,v} = 1$ .

$$\text{GSA}(K, V, Q) = \text{softmax}\left(\frac{1}{\sqrt{d_q}} \Gamma(Q, K)\right) G_v V \quad (5)$$

$$\text{with } \Gamma(Q, K) = \text{symmetric}\left(\sigma\left(G_{qk} \left(G_q Q \ [G_k K]^T\right) + G_b\right) \odot G\right).$$

only if the distance between the  $i^{\text{th}}$  and  $j^{\text{th}}$  vertex is the same.

**Rotational Symmetry.** To ensure that the layer solely possesses rotational symmetry, it is essential to disrupt the flip symmetry. This can be accomplished by selecting flip and rotational graph matrices, as depicted in fig. 2 (c), and summing over distinct directed subgraphs with three vertices, i.e., triangles, while assigning weights to each contribution see equation 7.

In essence, this implies that for any component of  $\Gamma(Q, K)_{\text{edge}}$ , two additional entries are added, all weighted with  $\Theta$ 's. The  $\Theta$ 's are trainable parameters, which will be shared if the angle between two edges of the triangle is identical.

In equation 4, the third vertex of the triangle is chosen as a function of  $i, j \mapsto k = T(i, j)$  for a unique map  $T$ ; the weights  $\Theta$ 's are shared if the angle between edges of the triangle in the square grid is identical. The label  $(i \rightarrow j \rightarrow k)$  denotes the angle at the  $j^{\text{th}}$  vertex i.e. between the  $(ij)$  and  $(jk)$  edge. In essence, this implies that for any of the  $P^2$ -components of  $\Gamma(Q, K)$ , two additional entries are added, all weighted with  $\Theta$ 's.

A unique triangulation of the square grid is chosen as follows. Disregarding the heads-dimension for the time being, any entry of the matrix  $\Gamma(Q, K)$  can be construed as a connection between a specific patch and another, thereby enabling the drawing of an edge from the former to the latter. This forms the initial directed edge of the triangle, linking two vertices. From the end of the latter, we opt to turn right

$$\begin{aligned}
 \text{GSA}_{\text{rot}}(K, V, Q) &= \text{softmax}\left(\frac{1}{\sqrt{d_q}} \sum_{\text{triangle edge} = 1}^{3P^2} \Theta_{\text{tri. edge}} \Gamma(Q, K)_{\text{tri. edge}}\right) V \\
 &= \text{softmax}\left(\frac{1}{\sqrt{d_q}} \Gamma^{\text{rot}}(Q, K)\right) V, \text{ where}
 \end{aligned} \tag{7}$$

$$\Gamma^{\text{rot}}(Q, K)_{ij} = \Theta^{(i \rightarrow j \rightarrow k)} \Gamma(Q, K)_{ij} + \Theta^{(j \rightarrow k \rightarrow i)} \Gamma(Q, K)_{jk} + \Theta^{(k \rightarrow i \rightarrow j)} \Gamma(Q, K)_{ki}, \tag{8}$$

and proceed to the nearest vertex in the grid, constituting the third vertex of the triangle. The direction of the edges is determined by traversing the triangle. Notably, as flips modify left/right and/or up/down, the aforementioned sum is not invariant under flips; however, it preserves left/right rotations, which transform the grid into itself.

**Duality to convolutional kernels.** See Figure (9) and (2) for a visualisation. The shared nature of the graph-matrix elements make them identical to a 2D-convolutional layer if the *kernel size* =  $2 * \text{image size} + 1$ , for a square image. If a specific kernel size is chosen it corresponds to the graph matrix with zero entries for vertices of larger distance than the kernel size, see Figure (9).

### A.1. One-dimensional Data / Sequential Data

While our discussion centers on the 2D grid, GSA may be adapted to 1D data where it ensures shift-symmetry and an optional flip-symmetry.

One may define  $G$  formally for the 1D case as. The data points in the 1D data are consider vertices, then assume that the distances are measured w.r.t. a specific vertex, and edges can be viewed as vectors. Then, pick  $G \in \mathbb{R}^{P \times P}$  such that a shared weight is present in  $G$ :

1. When horizontal component of edges have the same magnitude ( flip-preserving)
2. When the magnitude of the edges is same, but direction left/right i.e. the sign is accounted for which results in shift-symmetry.

Points (1) and (2) above are completely analog to the more complicated 2D case which is proofed in section E. Flip-preserving 1D GSA (1) for sequential data implements time-reversal symmetry, recently discussed in the context of RL (Cheng et al., 2023).

### Application of Transformers in RL on Sequence data:

The rise of Transformers in model-based RL (Chen et al., 2021; Micheli et al., 2023) opens up another direction which may adapt our approach.

## B. Overview: Symmetry-invariant Transformer

See Figure (3) for a schematic overview of the SiT architecture and for details on the symmetry of SiTs Figure 10. The local attention window's are processed by a GSA, which then passes only the token embedding dimension onto the global GSA layers. Since the token embedding dimension is invariant under the respective symmetries the global GSA receives a symmetry-invariant input of the local patches.

## C. Algorithm details

The implementation of the rotation symmetry breaking is a bit lengthy however straightforward. We omit details of how to compute the angles of triangles of vertices on the square grid, and just assert the function "rot\_grid\_to\_idx" here.

Lastly, in order to achieve scalability of SiTs we need to establish a connecting between graph matrices and depth-wise convolutions with graph-weights as kernels. The latter implementation is significantly more memory efficient. We note here that the below code is equivalent to multiplication of graph matrix given in Lisitng 1.

## D. GSA - Graph Symmetric Attention

In the following  $K$ ,  $V$ , and  $Q$  denote the keys, values, and queries respectively. They are derived from the input  $X$ :  $K = XW^k$ ,  $V = XW^v$ ,  $Q = XW^q$ , where  $W^q$ ,  $W^k$ , and  $W^v$  are the corresponding weight matrices, i.e.  $V_{ia} = \sum_{x=1}^{d_f} X_{ix} W_{xa}^v$ . The permutation invariant self-attention layer (Lee et al., 2019) is given by

$$\text{Att}(K, V, Q) = f(Q, K) X W^v \tag{9}$$

$$\text{with } f(Q, K) = \frac{1}{\sqrt{d_q}} \text{softmax}\left(Q [X W^k]^T\right),$$

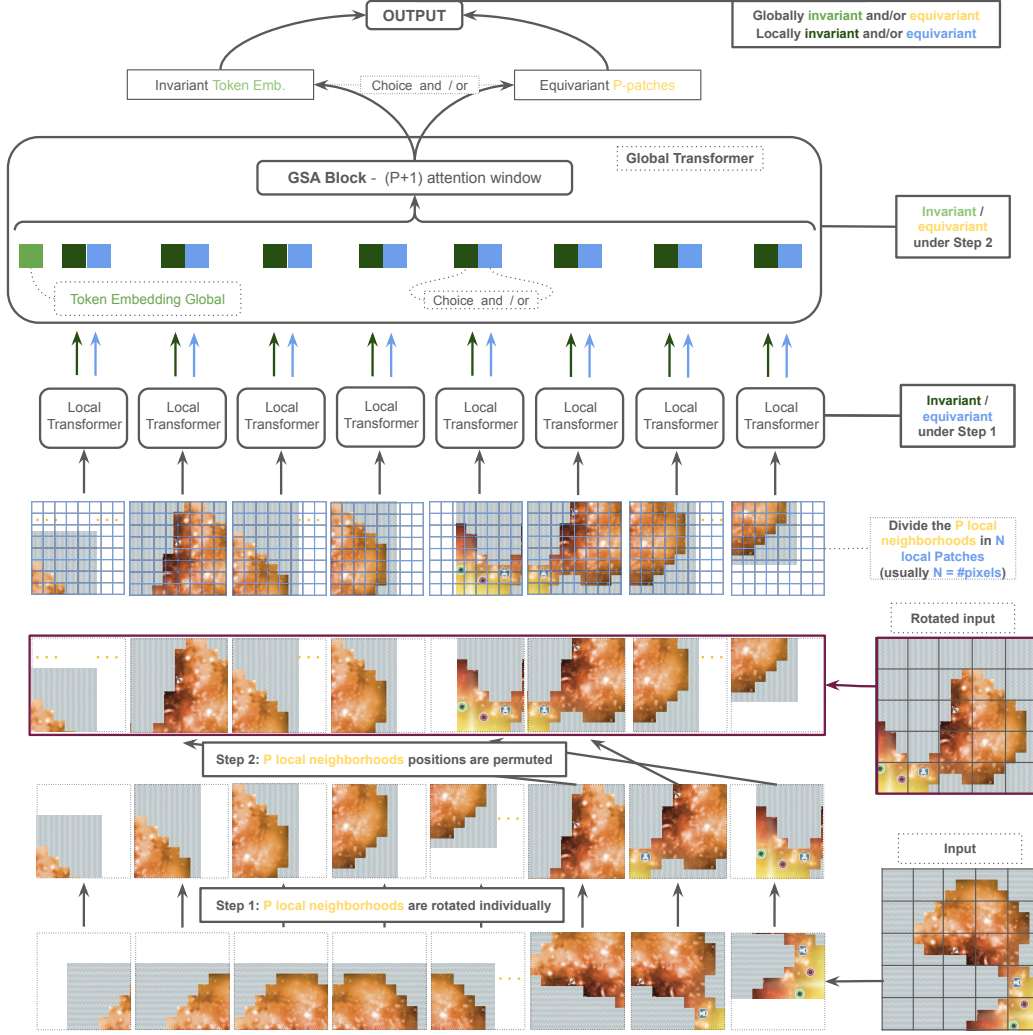


Figure 10. Illustration on exact global symmetries of SiTs; obtained as a result of the combined effect of local and global GSA modules.

which can be rewritten using explicit indices. One finds

$$Att(K, V, Q)_{qa} = \sum_{i=1}^P \text{softmax}\left(\frac{1}{\sqrt{d_q}} f(Q, K)_{qi}\right) V_{ia}$$

$$\text{with } f(Q, K)_{qi} = \sum_{a=1}^{\#heads} Q_{qa} [K]_{ai}^T, \quad (10)$$

For the original self-attention mechanism (Dosovitskiy et al., 2020) one simply needs to use a non-fixed  $Q = X W^q$  in equation 10 as

$$Att(K, V, Q)_{qa} = \sum_{i=1}^P \frac{1}{\sqrt{d_q}} \text{softmax}\left(f(Q, K)_{qi}\right) V_{ia}$$

$$\text{with } f(Q, K)_{qi} = \sum_{a=1}^{\#heads} Q_{qa} [K]_{ai}^T,$$

We propose the following three variants of Graph Symmetric Attention (GSAention) layer - all of which separately preserves the identical symmetries -

$$GSA(K, V, Q) = \text{softmax}\left(\frac{1}{\sqrt{d_q}} \Gamma(Q, K)\right) G_v V$$

$$\text{with } \Gamma(Q, K) = \text{symmetric}\left(G_q Q [G_k K]^T\right) \quad (11)$$

and

$$GSA(K, V, Q) = \text{softmax}\left(\frac{1}{\sqrt{d_q}} \Gamma(Q, K)\right) V \quad (12)$$

$$\text{with } \Gamma(Q, K) = \text{symmetric } \sigma\left(G_{qk} (Q [K]^T) + G_b\right),$$

and moreover

$$GSA(K, V, Q) = \text{softmax}\left(\frac{1}{\sqrt{d_q}} \Gamma(Q, K)\right) V W^v$$

$$\text{with } \Gamma(Q, K) = \text{symmetric}\left(Q [K]^T\right) \odot G,$$



```

class GraphSymmetricAttention(Module):
    def __init__(self, dim, num_patches, num_heads):
        self.num_heads = num_heads
        self.qkv = Linear(dim, dim * 3) # Fully-connected layer
        # Generate shareable graph weights
        self.G_weights, self.G_idxxs = graph_function(num_patches, dim * 3)

    def qkv_SymBreak(self, x):
        # Select indices of weights along dimension
        G = index_select(self.G_weights, 1, self.G_idxxs)
        # Matrix multiply with G; omit token embedding dimension
        y = G @ x[:, 1:, :]
        return cat([x[:, 0:1, :], y], dim=1)

    def forward(self, x):
        B, N, C = x.shape
        qkv = self.qkv_SymBreak(self.qkv(x))
        qkv = qkv.reshape(B, N, 3, self.num_heads, C // self.num_heads).permute(2, 0, 3,
1, 4)
        q, k, v = qkv[0], qkv[1], qkv[2]
        attn = (q @ k.transpose(-2, -1))
        # symmetric attention (if used)
        attn = attn + attn.transpose(-2, -1)
        attn = attn.softmax(dim=-1)
        return (attn @ v).transpose(1, 2).reshape(B, N, C)
    
```

Listing 1. Pseudocode for GSA (PyTorch-like). Changes relative to self-attention in brown.

```

def graph_function(num_patches, in_features):
    #compute simple distance of vertices in square grid
    for k in range(0, num_patches):
        for l in range(0, num_patches):
            for i in range(0, num_patches):
                for j in range(0, num_patches):
                    I = k * num_patches + l
                    J = i * num_patches + j
                    dist[I, J] = sqrt((k - i) ** 2 + (l - j) ** 2)

    #identify equal distances and associate unique index
    unique = dist.flatten().unique()
    dim = unique.shape[0]
    for i in range(dim):
        mask = (dist == unique[i])
        idxs[mask] = i
    #initialise independent weights
    weights = Parameter(Tensor(in_features, dim))
    return weights, idxs
    
```

Listing 2. Pseudocode for shared weight graph indices (PyTorch-like).

In index notation equation 11 results in equation 13. Moreover, equation 12 in detailed index notation is given by

$$\bar{\Gamma}(Q, K)_{qi} = \sigma \left( \sum_{a=1}^{\#heads} \sum_{j=1}^P G_{qkqj} Q_{ja} [K]_{ai}^T + G_{bqi} \right).$$

## E. Proofs of Invariance

Permutation matrices  $\mathcal{P}$  are orthogonal matrices. An orthogonal matrix is a square matrix whose transpose is equal to its inverse, i.e.  $\mathcal{P}^T = \mathcal{P}^{-1}$ . A permutation matrix is a square matrix obtained by permuting the rows and columns of an identity matrix. It represents a permutation of the elements in a vector or a rearrangement of the columns and rows of another matrix. Since permuting the rows and columns of an identity matrix results in swapping rows and columns,

```

class GraphSymmetricAttention(Module):
    def __init__(self, dim, num_patches, num_heads):
        self.rot_SymBreak = Rotation_Symmetry( num_patches, num_heads)

        # ... we only highlight the differnces in the forward pass

    def forward(self, x):
        B, N, C = x.shape
        qkv = self.qkv_SymBreak(self.qkv(x))
        qkv = qkv.reshape(B, N, 3, self.num_heads, C // self.num_heads).permute(2, 0, 3,
1, 4)
        q, k, v = qkv[0], qkv[1], qkv[2]
        attn = (q @ k.transpose(-2, -1))
        # symmetric attention (if used)
        attn = attn + attn.transpose(-2, -1)
        attn = self.rot_SymBreak(attn)
        attn = attn.softmax(dim=-1)
        return (attn @ v ).transpose(1, 2).reshape(B, N, C)

class Rotation_Symmetry(Module):
    def __init__(self, num_patches, num_heads):
        #compute unique angles of triangles in square grid
        idxs, idxs_angles, dim = rot_grid_to_idx(num_patches)
        self.idxs = idxs
        self.idxs_angles = idxs_angles
        #initialise independent weights
        self.angles = Parameter(Tensor(num_heads,dim))

    def forward(self, x):
        bs, heads, ps, ps= x.size()
        #index only non-token dimensions
        y = x[:, :, 1:, 1:].flatten(-2)[:, :, self.idxs]
        #preserve rotation/translation invariances, break flip invariances
        angles = index_select(self.angles, 1, self.idxs_angles.flatten())
        #multiply vertex with corresponding weight and sum over triangle
        y = (y*angles).reshape((bs, heads, ps-1, ps-1, 3)).sum(-1)
        #attach token dimension
        y = cat([ x[:, :, :, 0:1], cat([x[:, :, :, 0:1, 1:], y], dim=2)], dim=-1)
        return y.reshape(x.shape)

```

Listing 3. Pseudocode for GSA with rotation symmetry(PyTorch-like). Changes relative to self-attention in brown.

the transpose of a permutation matrix is equal to its inverse. Therefore, permutation matrices are orthogonal matrices.

The main theoretical claims of this work are summarized in proposition 3.1 , repeated here

**Proposition E.1 (Symmetry Guarantee)** *The GSA mechanism (equation 3) represents a symmetry-preserving module. It may be both invariant and/or equivariant w.r.t. symmetries of the input. The corresponding symmetry is dictated by the various graph selections. To achieve rotation invariance, the subsequent application of equation 4 is necessary. For invariance the token embedding i.e. the artificial ( $P-1$ )<sup>th</sup> patch is utilized at the output. Due to this mechanism, self-attention (equation 1) is permutation invariant. Equivariance is achieved for the  $P$ -dimensional patch information of the output, i.e. not related to the token embedding.*

First of all let us emphasise that we have implicitly empirically tested the validity of this claim in the various RL and supervised experiments in this work Let us discuss above claims in several steps:

**The attention mechanism equation 1 is permutation invariant (PI).** Let  $\mathcal{P}$  be a permutation of the input, i.e.  $Q, K, V \rightarrow \mathcal{P}Q, \mathcal{P}K, \mathcal{P}V$  as in equation 16. with  $[\mathcal{P} K]^T = K^T \mathcal{P}^T = K^T \mathcal{P}^{-1}$  and by using that the permutation matrix can be pulled out of the softmax-function as it is not affected by it results in equation 17. where we have used that  $\sum_{i=1}^P \mathcal{P}_{mi}^{-1} \mathcal{P}_{ij} = \delta_{mj}$ , where  $\delta$  is the Kronecker delta function, i.e. a formal way of writing the identity matrix. **We have showed that the attention mechanism is permutation equivariant. Invariance follows form the observation that when a token embedding is added it is not affected by the permutation matrix which only acts**

```

def graph_function(kernel_size):
    dist_Mat = torch.zeros((kernel_size, kernel_size))

    #only works correctly if kernel_size is odd
    i0, j0 = (kernel_size - 1) // 2, (kernel_size - 1) // 2
    for i in range(0, kernel_size):
        for j in range(0, kernel_size):
            distance = math.sqrt((i0-i)**2 + (j0-j)**2)
            dist_Mat[i, j] = distance

    unique = torch.unique(dist_Mat)
    idxs = torch.zeros(dist.shape)
    dim = unique.shape[0]
    for i in range(dim):
        mask = (dist == unique[i])
        idxs[mask] = i

    #initialise independent weights
    weights = Parameter(Tensor(in_features, dim))
    return weights, idxs

class GraphSymmetricAttentionEfficient(Module):
    ...
    def qkv_SymBreak(self, x):
        # Select indices of weights
        # of shape (in_features, 1, kernel_size, kernel_size)
        G = index_select(self.G_weights, 1, self.G_idx)
        # depthwise convlution with weights G; omit token embedding dimension
        y = conv2d(x, G, padding=(kernel_size-1)//2, groups=in_features)
        return y
    ...

```

Listing 4. Pseudocode for an efficient GSA (PyTorch-like). Changes relative to Listing (1) and (2) are presented.

on the patches. Thus it remains invariant as

$$Att(\mathcal{P}K, \mathcal{P}V, \mathcal{P}Q)_{q=P+1a} = Att(K, V, Q)_{q=P+1a} \quad (18)$$

**The graph symmetric attention mechanism equation 3 represents a symmetry-preserving, i.e. it can be both invariant and equivariant w.r.t. symmetries of the input. The corresponding symmetry is dictated by the various graph selections.** Let  $\mathcal{P}$  be a permutation of the input, i.e.  $Q, K, V \rightarrow \mathcal{P}Q, \mathcal{P}K, \mathcal{P}V$  then one finds equation 19. First of all note that since  $\mathcal{P}G - G\mathcal{P} \neq 0$ , i.e. they do not commute, thus GSA is not permutation equivariant (invariant).

**Definition 1 (Graph Matrix)** *The symmetric graph matrix  $G \in \mathbb{R}^P \times \mathbb{R}^P$  are defined as having a shared weight at entry  $G_{ij} = G_{ji}$  if*

- the distance of the  $i$ -vertex to the  $j$ -vertex in the square grid of the 2D-image have same length. This leads to a flip and rotation invariant graph matrix.

- the horizontal distance of the  $i$ -vertex to the  $j$ -vertex are the same, and the vertical distance is zero. This leads to a horizontal mirror flip graph.

Thus a permutation  $\mathcal{P}^s$  does commute with the graph matrix if and only if it maps shared weights of  $G$  to each other; then  $\mathcal{P}^s G - G\mathcal{P}^s = 0$ . Then one can rewrite the above expression as in equation 21. The remaining steps are analog to the one for the conventional attention which is concluded in equation 22. **which states the equivariance of GSA and invariance when a token embedding is used at dimension  $P + 1$  with respect to the symmetry preserving permutation  $\mathcal{P}^s$ .**

Two remaining points are twofold. First, the derivation above holds in particular for the symmetrisation (anti-symmetrisation) of  $\Gamma$ . Second, to see that graphs matrices with particular choices of shared weights lead to the desired symmetries of the 2D-grid we refer the reader to a visual proof given in figure 2. The proof of equivariance for the setting with  $G_{kq}, G_b$  is analog. The case for  $G$  one notes that a  $P \times P$ -matrix  $\sum_{i=1}^P \mathcal{P}_{ki}^s M_{ij} * G_{ij} = M_{ij} * G_{ij}$  if and only if  $\mathcal{P}^s$  only permutes shareable weights of the graph

$$GSA(K, V, Q)_{qa} = \sum_{i=1}^P \frac{1}{\sqrt{d_q}} \text{softmax}\left(\Gamma(Q, K)_{qi}\right) \sum_{j=1}^P G_{vij} V_{ja} \quad (13)$$

$$\text{with } \bar{\Gamma}(Q, K)_{qi} = \sum_{a=1}^{\#heads} \sum_{k=1}^P G_{qk} Q_{ka} \sum_{j=1}^P G_{kij} [K]_{aj}^T, \quad (14)$$

$$\Gamma(Q, K)_{ij} = \bar{\Gamma}(Q, K)_{ij} + \bar{\Gamma}(Q, K)_{ji}. \quad (15)$$

$$Att(\mathcal{P}K, \mathcal{P}V, \mathcal{P}Q)_{qa} = \sum_{i=1}^P \text{softmax}\left(\frac{1}{\sqrt{d_q}} \Sigma(\mathcal{P}Q, \mathcal{P}K)_{qi}\right) \sum_{j=1}^P \mathcal{P}_{ij} V_{ja} \quad (16)$$

$$\text{with } \Sigma(\mathcal{P}Q, \mathcal{P}K)_{qi} = \sum_{a=1}^{\#heads} \sum_{l=1}^P \mathcal{P}_{ql} Q_{la} \left[ \sum_{j=1}^P \mathcal{P}_{ij} K \right]_{aj}^T,$$

$$\begin{aligned} Att(\mathcal{P}K, \mathcal{P}V, \mathcal{P}Q)_{qa} &= \sum_{i=1}^P \sum_{l=1}^P \mathcal{P}_{ql} \left( \frac{1}{\sqrt{d_q}} \text{softmax} \Sigma(Q, K)_{lm} \right) \sum_{m=1}^P \mathcal{P}_{mi}^{-1} \sum_{j=1}^P \mathcal{P}_{ij} V_{ja} \\ &= \sum_{j=1}^P \sum_{l=1}^P \mathcal{P}_{ql} \text{softmax}\left(\frac{1}{\sqrt{d_q}} \Sigma(Q, K)_{lj}\right) V_{ja} \\ &= \sum_{l=1}^P \mathcal{P}_{ql} Att(K, V, Q)_{la} \end{aligned} \quad (17)$$

$$GSA(\mathcal{P}K, \mathcal{P}V, \mathcal{P}Q)_{qa} = \sum_{i=1}^P \text{softmax}\left(\frac{1}{\sqrt{d_q}} \Gamma(\mathcal{P}Q, \mathcal{P}K)_{qi}\right) \sum_{j=1}^P G_{vij} \sum_{l=1}^P \mathcal{P}_{lj} V_{ja} \quad (19)$$

$$\text{with } \Gamma(\mathcal{P}Q, \mathcal{P}K)_{qi} = \sum_{a=1}^{\#heads} \sum_{k=1}^P G_{qk} \sum_{l=1}^P \mathcal{P}_{km} Q_{ma} \sum_{j=1}^P G_{kij} \sum_{l=1}^P \mathcal{P}_{jl} [K]_{al}^T, \quad (20)$$

$$GSA(\mathcal{P}^s K, \mathcal{P}^s V, \mathcal{P}^s Q)_{qa} = \sum_{i=1}^P \text{softmax}\left(\frac{1}{\sqrt{d_q}} \Gamma(\mathcal{P}^s Q, \mathcal{P}^s K)_{qi}\right) \sum_{l=1}^P \mathcal{P}_{il}^s \sum_{j=1}^P G_{vlj} V_{ja}$$

$$\text{with } \Gamma(\mathcal{P}^s Q, \mathcal{P}^s K)_{qi} = \sum_{a=1}^{\#heads} \sum_{l=1}^P \mathcal{P}_{qk}^s \sum_{k=1}^P G_{qkm} Q_{ma} \sum_{l=1}^P \mathcal{P}_{ij}^s \sum_{j=1}^P G_{kjl} [K]_{al}^T, \quad (21)$$

$$GSA(\mathcal{P}^s K, \mathcal{P}^s V, \mathcal{P}^s Q)_{ia} = \sum_{l=1}^P \mathcal{P}_{ij}^s GSA(K, V, Q)_{ja} \quad (22)$$

$$GSA(\mathcal{P}^s K, \mathcal{P}^s V, \mathcal{P}^s Q)_{i=P+1a} = GSA(K, V, Q)_{i=P+1a} \quad (23)$$

matrix, i.e. thus  $\mathcal{P}^s$  needs to obey the symmetry properties. The rest of the steps to conclude the proof are analog as above.

**To achieve rotation invariance, the subsequent application of equation 4 is necessary.** Let  $\Gamma_{ij}$  be graph  $P \times P$ -matrix obeying rotation and flip symmetries of an underlying square grid, and let  $\mathcal{T}(i, j) \mapsto k$  be unique mapping for every tuple  $(i, j)$  to the vertex  $k$ ; i.e. such that  $(i, j, k)$  forms a triangle in the grid. Moreover  $\mathcal{T}$  is such that the angles of the resulting triangle only depend on the distance between i-j., and the orientation in clock-wise starting from  $i \rightarrow j \rightarrow k \rightarrow i$ . The weights  $\Theta(ij, jk)$  are shared if the angles in the triangle are equal.

$$\Gamma^{\text{rot}}(Q, K)_{ij} = \Theta^{(i \rightarrow j \rightarrow k)} \Gamma(Q, K)_{ij} \quad (24)$$

$$+ \Theta^{(j \rightarrow k \rightarrow i)} \Gamma(Q, K)_{jk} + \Theta^{(k \rightarrow i \rightarrow j)} \Gamma(Q, K)_{ki} ,$$

The notation is such that  $\Theta^{(i \rightarrow j \rightarrow k)}$  means corresponding to the angle between the edges i-j and j-k. Then we may rewrite the expression from the main text more concisely as where  $\mathcal{T}(i, j) = k$ . Any transformation which maps equal distance edges to each other will leave  $\Gamma(Q, K)_{ij}, \Gamma(Q, K)_{jk}, \Gamma(Q, K)_{ki}$  invariant, respectively. However more specifically flip transformation change the meaning of clock-wise and anti-clockwise and thus

- $\Theta^{(i \rightarrow j \rightarrow k)} \mapsto \Theta^{(k \rightarrow i \rightarrow j)}$ ,
- $\Theta^{(j \rightarrow k \rightarrow i)} \mapsto \Theta^{(j \rightarrow k \rightarrow i)}$ ,
- $\Theta^{(k \rightarrow i \rightarrow j)} \mapsto \Theta^{(i \rightarrow j \rightarrow k)}$ .

Thus equation 25 does not preserve flip transformation. While rotations leave the  $\Theta$ 's invariant. This concludes the proof of the proposition.

## F. Hyper-parameters - Main Experiments

### F.1. Minigrid - Lavacrossing

We employ our invariant SiTs on top of IMPALA (Espeholt et al., 2018) implementation based on torchbeast (Küttler et al., 2019). For the experiments involving SiTs and ViTs, we do not employ any hyper-parameter tuning compared to the CNN baseline (Jiang et al., 2021) - hyperparameters can be found in that reference. We use the stated number of local and global GSA with an embedding dimension of 64 and 8 heads. The attention window of the global GSA is the entire image, i.e  $14 \times 14$  (pixels) which corresponds to  $P = 196$  patches ; while locally we choose patch-size of 5 (pixels), i.e. a attention window of  $5 \times 5$  (pixels) or  $P = 25$  patches. We use rotation invariant GSA both on the local as well as on the global level.

While, MiniGrid environments are partially observable by default we configure our instances to be fully observable; as well as change the default observation size  $9 \times 9$  pixel to  $14 \times 14$  pixel. The latter is done by rendering the environment observation and then down-scaling to the respective size. Moreover, the default action space only allows the agent to turn left, turn right, or move forward, which requires the agent to keep track of its direction while navigating. To make the environment more accessible , we modify the action space, enabling the agent to move in all four candidate directions i.e. to move left, right, forward and backward.

For Minigrid, we selected a  $14 \times 14$  global image size as this is the minimum resolution at which the direction of the triangular shaped agent can be discerned when downscaling the RGB rendering of the environment. Smaller resolutions fail to capture this detail, while larger ones are feasible but not necessary. The local neighborhood size in Minigrid (in pixels) is required to be odd, so  $3 \times 3$  and  $5 \times 5$  are the smallest viable options.

**Architecture Details.** For the CNN baseline, we use two convolutions layers two fully connected ones. The ViT and SiT and architectures both employ a skip connection  $x \rightarrow x + \text{Att}(x)$  and  $x \rightarrow x + \text{GSA}(x)$ , respectively. As in (Beyer et al., 2022), we modify the Vi architecture of (Dosovitskiy et al., 2020) by not using a multi-layer perceptron (MLP) after each attention layer. Our goal is to encounter the most simple functional setting incorporating the attention mechanism. We use one embedding fully-connected layer and use a patch-embedding. We employ our invariant SiTs on top of IMPALA (Espeholt et al., 2018) implementation based on torchbeast(Küttler et al., 2019). For the experiments involving SiTs and ViTs, we do not employ any hyper-parameter tuning compared to the CNN baseline (Jiang et al., 2021). Qualitatively, even when trying to tune ViTs by running a hyper-parameter sweep, we could not improve their performance by more than a factor of two.

### F.2. Procgen experiments

We train with PPO (DrAC) + Crop augmentation for SiT (Sit\*, Set, Siet) and compare to the CNN (ResNet with model size  $79.4k$  comparable to the SiT -  $65.7k$ ; ViT with 4-layers -  $216k$  ). For parameter details see table (2).

We do not alter the ResNet architecture of (Raileanu et al., 2020) but chose the same hidden-size of 64 as for the SiT as well reduce the number of channels to  $[4, 8, 16]$ . We train over 25M steps. Following Agarwal et al. (2021b), we report the min-max normalized score that shows how far we are from maximum achievable performance on each environment. All scores are computed by averaging over both the 4 seeds and over the 23M-25M test-steps. We also report UCB-DrAC results with Impala-CNN( $\times 4$ ) ResNet with 620k parameters, taken from (Raileanu et al., 2020).

### F.3. DM control

We train SieT - Without any hyper-parameter and backbone changes compared to our Procgen setup - with SAC (Haarnoja et al., 2018) for 500k steps. No data-augmentation is used. SieT has comparable performance to the ViT baseline with  $> 1M$  weights (Hansen & Wang, 2021). For parameter details see table (2).

### F.4. Proof of sample-efficiency: Atari 100k

The Atari 100k benchmark (Kaiser et al., 2020), comprising 26 Atari games (Bellemare et al., 2013), spans various mechanics and evaluates a broad spectrum of agent capabilities. In this benchmark, agents are restricted to 100k actions per environment, approximating 2 hours of human gameplay. For context, typical unconstrained Atari agents undergo training for 50 million steps, signifying a 500-fold increase in experience.

Current standards in Atari 100k for search-based methods include MuZero (Schrittwieser et al., 2020) and EfficientZero (Ye et al., 2021), and recently a transformer based world-model approach (Micheli et al., 2023). Image-based SiTs may compliment those methods. In particular the latter may benefit from GSA, see our discussion in section A.1. We just provide a proof-of concept for using shift symmetric GSA instead of positional embedding in the world-model transformer of IRIS (Micheli et al., 2023).

See Figure 11 for the results on KungFuMaster averaged over a hyper-parameter search for varying world-model training steps for 7 runs for values in  $[50, 200]$  (with default of 200). This illustrates the hyper-parameter insensitivity of GSA and suggests improved sample-efficiency over positional embedding.

**Sample-efficiency:** See Figure 12 and Figure 13 for results on KungFuMaster and MsPacMan, respectively. Here we have replaced the CNN in the actor by a smaller SieT model with 1 local and 2 global layers. To speed up training we have reduced the number of local features to 32 (64 global features). One infers that although the final training performance is lower than the one obtained by the baseline (IRIS + CNN) that IRIS + SieT is sample efficient, i.e. it reaches its peak quite early in training within 200 epochs which corresponds to about 40k exploration steps. Note that we have only tested one SieT model and performed no hyper-parameter search. The goal here is not to improve on Iris which had optimized h-parameters for their CNN actor model but to show that SieT admits the capability to learn from a small sample size; which is inferred from Figure 12 and Figure 13.

Our goal here is not to show a comparison to state-of-the-art on Atari 100k in terms of sample-efficiency but that SiTs may be trained with ease on-top of standard algorithms.

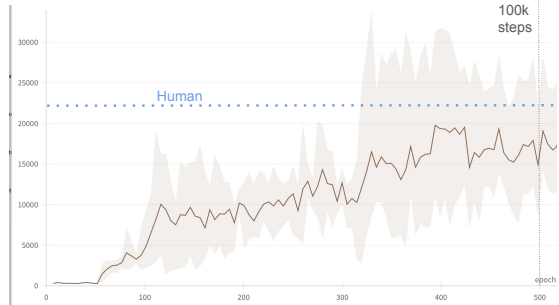


Figure 11. Results on KungFuMaster with 1D GSA in (Micheli et al., 2023) averaged over a hyper-parameter search for varying world-model training steps in  $[50, 200]$  (with default of 200). 500 Epochs correspond to 100k exploration steps.

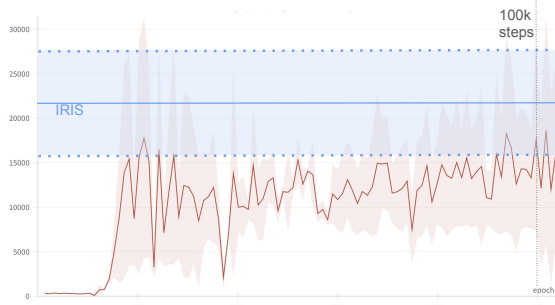


Figure 12. Results on KungFuMaster with SieT in actor instead of CNN in (Micheli et al., 2023), averaged over 3 seeds. The IRIS performance after 100k steps is marked by a blue horizontal bar.

Thus, for our Atari 100k experiments we **use the unchanged hyper-parameter setting of Rainbow (Hessel et al., 2017)**, both for the baseline model - data-efficient CNN - as well as the algorithm for both CNN and our SieT. The SieT model is the same as in the Procgen experiments but with one less local GSA layer and increased embedding dimension, see Table 2. **The baseline CNN has approximately 3x more weights than SieT. See Figure 14 for example training curves.**

### F.5. Technical improvements

Moreover, another minor modification to the architecture lead to a compute speed-up, which is not to use a token embedding in the local attention layer but rather use a depth wise graph-like convolution with kernel-size and stride equal to the patch-size as a last layer. This is common practice for ViTs i.e. by using normal convolutions that way. It is easy to see that our choice also preserves the symmetries of the graph-matrix. So, concludingly using a token embedding is not the only architectural choice which leads to a preservation of symmetries in SiTs.

First, we establish a connection between graph matrices

Suite / Algorithm	Model	Layers	Channels	Hidden dim.
Procgen (Raileanu et al., 2020)	CNN	3 ResNet (Raileanu et al., 2020)	[4,8,16]	64
	ViT	4 Attn. Layers (Hansen & Wang, 2021)	64	64
	E2CNN	4 E2CNN Layers (Wang et al., 2022a)	[2,4,8,8]	64
	E2CNN'	4 E2CNN Layers (Wang et al., 2022a)	[2,4,8,16]	64
	SiT	2 local GSA, 2 global GSA	64	
	SiT*	2 local GSA, 2 global GSA	64	64
	SeT	2 local GSA, 2 global GSA	64	64
	SieT	2 local GSA, 2 global GSA	64	64
	UCB-CNN	3 ResNet (Raileanu et al., 2020)	[16,32,32]	256
DM-control (Hansen & Wang, 2021)	SieT	2 local GSA, 2 global GSA	64	64
Atari 100k (Hessel et al., 2017)	CNN	data-efficient (Hessel et al., 2017)	[32,64] (approx. 880k)	256
	SieT	1 local GSA, 2 global GSA	128 (approx. 309k)	256

Table 2. Architecture and hyper-parameter choices for Procgen and DM-control. UCB-CNN is taken from (Raileanu et al., 2020). All SiT variants contain one initial conv. layer with shared graph weights and a subsequent max. pooling layer to reduce the dimensionality of the problem. For the Atari experiments, we use the unchanged hyper-parameter setting of Rainbow (Hessel et al., 2017).

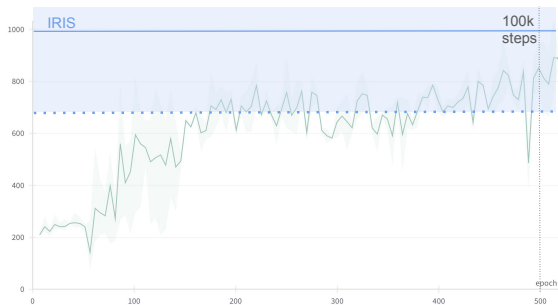


Figure 13. Results on MsPacMan with SieT in actor instead of CNN in (Micheli et al., 2023), averaged over 3 seeds. The IRIS performance after 100k steps is marked by a blue horizontal bar.

and depth-wise convolutions with graph-weights as kernels. The latter implementation is significantly more memory efficient and faster. Secondly, in order to accommodate for an extend local attention window we do use a graph matrix which connects pixels over larger distances while keeping the actual attention-mechanism focused on a smaller patch.

Thirdly, rather trivially one may scale down the original image size from  $64 \times 64$  pixels to  $32 \times 32$ . This can be done by simple scaling the image, or by using one initial depth-wise convolutional layer with graph-like weights to preserve symmetry plus a subsequent Max-Pooling operation, or by simply using every second pixel of the input-image.

Given the dominance of ViTs in Vision and Transformers in NLP, it’s plausible that improvements in Transformer technology will similarly revolutionize vision-based RL, with ViTs becoming predominant. Recent technical advancements, such as efficient Transformers (Dao et al., 2022), which offer up to a 10x performance boost may lead the way to a brad adaption of SiTs in RL. As the latter ensures that

Rainbow - data-efficient		
Atari Game	CNN	SieT
SpaceInvaders	344	366.3
BreakOut	4.3	4.97
Pong	-19.07	-20.04

Table 3. CNN vs. SiTs on Atari 100k benchmark environments: SpaceInvaders, BreakOut, Pong. We train with Rainbow (Hessel et al., 2017) and compare to the data-efficient CNN ( $\approx 880k$  weights ) about  $3\times$  larger than our SieT -  $\approx 309k$ . The number model parameters vary for different environments, however the factor in between CNN baseline and SieT is consistently  $\approx 3\times$ . We present absolute scores, averaged over evaluation after 80k,90k,100k train-steps and 3 seeds, respectively.

our sample efficient symmetry-invariant vision transformer becomes rather light-weight.

**CIFAR10 - supervised ablation study:** For the baseline we use a ViT (Dosovitskiy et al., 2020) , embedding dimension of 512, 4 layers, 16 heads, and one local attention layer with the same settings. The SiT has a the graph matrix  $G$  added.

## G. Additional Experiments and Ablations

### G.1. Ablation: Local and Global Symmetries in Attention for Image Understanding

In this section we present an ablation study which addresses the impact of local attention fields in SiTs, see results in Figure 15. For the performance comparison of the attention mechanism with both symmetrisation and anti-symmetrisation (Equation 6) in SiTs, we restrict ourselves to provide qualitative results. Performing several experi-

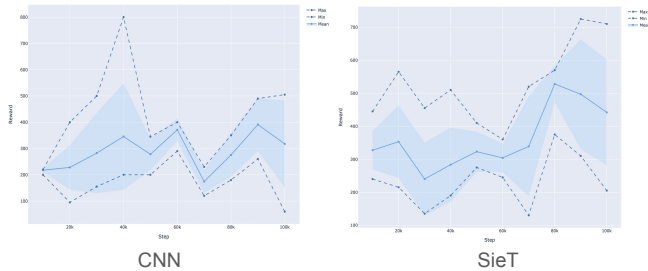


Figure 14. Example evaluation curves of Rainbow during training of SpaceInvaders seed 124 on top of rainbow - data efficient -.

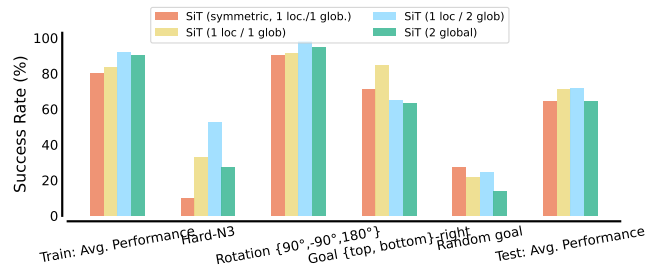


Figure 15. Ablations study SiT for different number of local and global layers as well as using the symmetric part of SiT\*, defined in the appendix.

ments with two global layers, of either symmetrisation and anti-symmetrisation or both present, we conclude that indeed the later admits the best relative performance as well as generalisation to the hard task, of all SiT setup with only global layers. However, due to the second softmax in the attention it is more memory consuming and thus applying it in combination with a the local layers is not feasible. Memory efficient attention mechanism (Dao et al., 2022) have been developed recently thus our better architecture may become technically available in the future.

Finally, we compare the impact of the employment of graph matrices in the values of the attention mechanism. We set  $G_v = 1$  and use one local and two global symmetric attention modules (Equation 6) with rotation invariance, see Figure 16. The graph matrix  $G_v$ , leads to a decrease in generalisation performance on goal change tasks and an increase in performance on the difficult environment involving many lava-crossings. Conceptually, the graph-matrix  $G_v$ , admits some similarities to convolutions, which are known to preform better on limited sample size (Hassani et al., 2022). Thus it may be easier for this architecture to identify two-dimensional information while setting it to the identity restores some degree of permutation invariance.

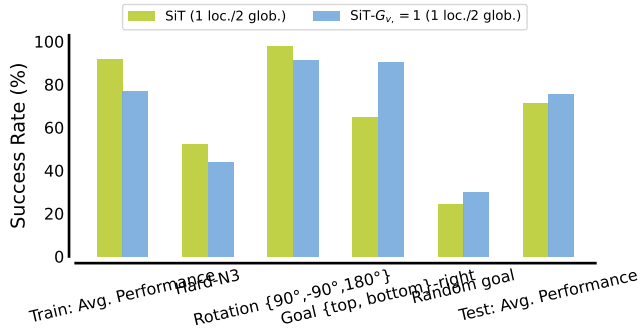


Figure 16. Ablations for using the symmetric part of SiT\*, defined in the appendix. We ablate by  $G_v$ , by setting  $G_v = 1$  with one local and two global symmetric attention modules equation 6 and rotation invariance.

## G.2. Minigrid - Lavacrossing

In this section we briefly provide the details with error bars to the experiment provided in the main text. The tables 4, 5 contain the mean rewards averaged over 200 test episodes after 20M time-steps.

## H. Additional Evaluations & Ablations

### H.1. Patch-size Ablation on CIFAR 10

In this section, we perform an ablation study on the sensitivity of SiT (Siet) to the patch-size hyper-parameter. In contrast to the evaluation of Figure (7b) here we employ a much smaller and faster model with 4 local and 4 global GSA layers and have reduced the feature dimensions to 64 and 256, respectively.

We perform an ablation study of varying patch-size of SieT model on CIFAR10 with resolution of 32x32 and 128x128 pixels, see Tables (6) and (7), respectively. Additionally, we vary the dimension of the graph matrix in the local GSA for fixed patch-size in selected cases. We conclude that SieTs can be applied without loss of accuracy performance to higher-resolution tasks and moreover are relatively insensitive to changes in the patch-size (Beyer et al., 2023).



Table 4. Details main results for the experiment on the Lavacrossing Minigrid environment.

Domain Train	Test Task	CNN	ViT	PI-ViT	SiT	SiT-1
Lavacrossing N1 & N2 medium & easy	<i>train: easy-N1</i>	0.96 ± 0.01	0.23 ± 0.41	0.01 ± 0.0	0.94 ± 13.0	0.90 ± 0.23
	<i>train: medium-N2</i>	0.69 ± 0.43	0.25 ± 0.42	0.01 ± 0.0	0.84 ± 0.32	0.70 ± 0.42
	hard-N3	0.54 ± 0.47	0.19 ± 0.38	0.01 ± 0.0	0.46 ± 0.48	0.41 ± 0.47
	rotations average	0.00 ± 0.00	0.15 ± 0.34	0.01 ± 0.0	0.91 ± 0.21	0.91 ± 0.22
	goal top-right	0.08 ± 0.27	0.21 ± 0.40	0.01 ± 0.0	0.71 ± 0.44	0.90 ± 0.24
	goal bottom-left	0.08 ± 0.25	0.20 ± 0.40	0.01 ± 0.0	0.71 ± 0.44	0.90 ± 0.24
	random goal	0.07 ± 0.25	0.15 ± 0.35	0.01 ± 0.0	0.24 ± 42.0	0.21 ± 0.40

Table 5. Ablation study for SiT with different numbers of local and global layers as well as using the symmetric part of SiT\*, defined in the appendix.

Train	Test Task	ViT		SiT			
		2 global	1 loc./2 glob.	symmetric 1/1	1 loc./1 glob.	1 loc./2 glob.	2 global
Lavacr. N1/N2	<i>train: easy-N1</i>	0.08 ± 0.27	0.23 ± 0.41	0.86 ± 0.29	0.90 ± 0.23	<b>0.93 ± 18.0</b>	0.87 ± 0.28
	<i>train: medium-N2</i>	0.12 ± 0.31	0.25 ± 0.42	0.88 ± 0.26	0.70 ± 0.42	0.84 ± 0.32	0.59 ± 0.46
	hard-N3	0.10 ± 0.29	0.19 ± 0.38	0.45 ± 0.43	0.41 ± 0.47	0.46 ± 0.48	0.03 ± 0.16
	rotations avg.	0.03 ± 0.16	0.15 ± 0.34	0.88 ± 0.27	<b>0.91 ± 0.22</b>	<b>0.95 ± 0.10</b>	0.91 ± 0.21
	goal top-right	0.03 ± 0.15	0.21 ± 0.40	0.81 ± 0.35	<b>0.90 ± 0.24</b>	<b>0.71 ± 0.44</b>	0.60 ± 0.48
	goal bottom-left	0.02 ± 0.13	0.20 ± 0.40	0.81 ± 0.35	<b>0.90 ± 0.24</b>	<b>0.71 ± 0.44</b>	0.60 ± 0.48
	random goal	0.08 ± 0.27	0.15 ± 0.35	<b>0.26 ± 0.43</b>	<b>0.21 ± 0.40</b>	<b>0.28 ± 0.44</b>	0.12 ± 0.32

Table 6. CIFAR 10 - 32x32 Results. Ablation study of varying patch-size of SieT model on CIFAR10 with resolution of 32x32 pixels. Additionally, we vary the dimension of the graph matrix in the local GSA, see x-axis. Gray bars indicate non-available cases, i.e. the combination of graph-matrix size with patch-size has not been conducted.

GSA Layers	Patch-Size Global	Patch-Size Local	Graph Matrix Size	Batch-Size	Test Accuracy 25 Epochs	Test Accuracy 200 Epochs
4loc-4glob	8x8	4x4	8x8	64	66%	-
4loc-4glob	4x4	8x8	16x16	64	62%	-
4loc-4glob	16x16	2x2	4x4	64	66%	-
4loc-4glob	4x4	8x8	8x8	64	58%	75%
4loc-4glob	16x16	2x2	8x8	64	67%	81%
4loc-4glob	8x8	4x4	6x6	64	65%	-
4loc-4glob	8x8	4x4	8x8	64	66%	-
4loc-4glob	8x8	4x4	12x12	64	66%	-

Table 7. CIFAR 10 - 128x128 Results. Ablation study of varying patch-size of SieT model on CIFAR10 with resolution of 128x128 pixels. The images are scaled up using AI tools [CIFAR-10 128x128](#). Additionally, we vary the dimension of the graph matrix in the local GSA, see x-axis. Gray bars indicate non-available cases, i.e. the combination of graph-matrix size with patch-size has not been conducted.

GSA Layers	Patch-Size Global	Patch-Size Local	Graph Matrix Size	Batch-Size	Test Accuracy 25 Epochs	Test Accuracy 15 Epochs
4loc-4glob	8x8	16x16	16x16	48	66%	63%
4loc-4glob	8x8	16x16	32x32	48	69%	64%
4loc-4glob	8x8	16x16	64x64	48	69%	64%
4loc-4glob	8x8	16x16	32x32	16	70%	66%
4loc-4glob	4x4	32x32	64x64	8	69%	66%